Polymeric Nanoparticles for Ultrasonic Enhancement and Targeted Drug Delivery

Thesis

Presented in Partial Fulfillment of the Requirements for the Degree Master of Science in the Graduate School of The Ohio State University

By

Jie Li

Graduate Program in Biomedical Engineering

The Ohio State University

2010

Thesis Committee:

Dr. Jun Liu, Advisor

Dr. Ronald Xu

Copyright by

Jie Li

2010

Abstract

Our previous studies have demonstrated ultrasonic enhancement *in vitro* via targeted polylactic acid (PLA) nanoparticles that selectively bound to surface receptors of breast cancer cells by using high frequency ultrasound. In this study, we aim to (1) test the feasibility of using polymeric nanoparticles for ultrasonic enhancement of tumor xenografts in mice through high frequency ultrasound system; (2) validate the nanoparticle enabled ultrasonic enhancement using diagnostic frequency ultrasound ex vivo and in vivo; and (3) develop multifunctional polymeric nanoparticles as a combined platform for ultrasound contrast enhancement and drug delivery. For Aim 1, nude mice were implanted with human breast cancer xenografts using cell lines of either MCF-7/HER2-18 (overexpressing HER2 receptors) or MDA-MB-231 (expressing HER2 at a low level). Tumors from each type were treated with anti-HER2 antibody-conjugated PLA nanoparticles via subcutaneous injection at the tumor site, or the same volume of PBS. All tumors were imaged with a high frequency ultrasound system at baseline, and 5, 15, 30 min, and 1 h post-treatment. A significant increase in ultrasonic reflectivity was observed in MCF-7/HER2-18 tumors after particle treatment (but not after PBS treatment) at 5, 15, and 30 min. No change was observed in the MDA-MB-231 tumors, suggesting that the ultrasonic enhancement may be mediated by specific binding of the surface conjugated nanoparticles to HER2 overexpressing tumor cells. For Aim 2, mouse livers were used for ex vivo study. SkBr3 human breast cancer cells (overexpressing

HER2 receptors) treated with anti-HER2 antibody-conjugated PLA nanoparticle were injected into mouse livers, and the same dosage of SKBr3 cells treated with PBS only was injected into mouse livers as control. HER2/neu transgenic mice were used for in vivo study and the conjugated particles or PBS was injected subcutaneously close to the tumors. All ultrasound images were acquired by clinic ultrasound system with a 14 MHz probe. The acoustic intensities within the injection area pre- and post-injection were quantified by ImageJ software. Consistently to the results from high frequency ultrasound imaging, the acoustic intensity only increased within the injection site of targeted PLA nanoparticles treated tumor cells or tumors. The maximal acoustic intensity was reached at 15 minutes after the injection in vivo. For Aim 3, a series of PLGA nanoparticles of various sizes (150, 300 and 500 nm) were fabricated by modified solvent-replacement method. Fluorescent probe was encapsulated into the nanoparticles as model drug and for tracking the nanoparticles. The targeting specificity and the resultant ultrasound enhancement were determined by fluorescent microscopy and high-resolution ultrasound imaging. The drug delivery efficiency of engineered nanoparticles was determined by observation of localization of nanoparticles in the cells via the confocal microscopy. SkBr3 cells demonstrated substantial staining after incubation with all sizes of nanoparticle/antibody conjugates, while no staining was found in MDA-MB-231 cells, indicating receptor-specific binding of the conjugated PLGA nanoparticles. In high-resolution ultrasound B-mode images, the average gray scale of the SkBr3 cells was significantly higher after 300 nm and 500 nm nanoparticle treatment than 100 nm nanoparticle treatment. In drug delivery study, the SkBr3 cells treated with antibody-

conjugated PLGA nanoparticles of 150 nm and 300 nm demonstrated sufficient intracellular localization, while minimal intracellular localization was detected in the cells that treated with 500 nm nanoparticles. These results indicated the feasibility of using polymeric nanoparticles (PLA and PLGA) for enhanced ultrasound imaging of tumors with both high frequency and diagnostic ultrasound. Biodegradable polymeric nanoparticles may be potential agents for combined ultrasound molecular imaging and targeted drug delivery. Considering both echogenicity and drug delivery efficiency, PLGA nanoparticles of 300 nm may be the most promising candidate based on the results in this study.

Dedication

This document is dedicated to my son Dudu.

Acknowledgments

While pursuing my graduate education, I received assistance from many individuals. First and foremost, I thank my husband, Dr. Tongzheng Liu. Without his encourage and support, my Master Program would not have been nearly fulfilling.

I am especially grateful to my advisor, Dr. Jun Liu for her guidance and support. I would also like to thank Dr. Ronald Xu for agreeing to be the committee member in my Master Program and his assistance in use of equipments.

I thank my colleagues – Xiaoyin He and Junhua Tang for their suggestion and encouragement. I also thank Dr. Jeff Xu for helping with fluorescence microscopy and Dr. Yun Wu for her helping with nanoparticle characterizations.

I thank Andrei Maiseyeu, PhD, Heart and Lung Research Institute, The Ohio State University, for his assistance with immunofluorescence staining; Xueliang Pan, PhD, Center for Biostatistics, The Ohio State University, for his assistance with statistical analysis; Pengfei Zhang, MD, Qilu Hospital of Shandong University, for his assistance in equipment and image processing; and Hui Wang, PhD, Comprehensive Cancer Center, The Ohio State University, for his assistance with transgenic mice.

Vita

1999.....B.S. Pharmacy, Shandong Medical University, Jinan, China

2001.....Research Associate, R&D department of Bausch&Lomb Freda Pharmacy Co.Ltd., Jinan, China

2004.....M.S. Cytobiology, National Lab of Molecular Oncology, Cancer Institute, Chinese Academy of Medical Sciences and Peking Union Medical College, Beijing, China

2008.....Research Associate, Department of Biomedical Engineering, the Ohio State University, Columbus, OH

2008 to present .....Graduate Research Associate, Department of Biomedical Engineering, the Ohio State University, Columbus, OH

Publications

Journals

1. **Jie Li** and Jun Liu. Targeted nanoparticles for enhanced ultrasound imaging of HER2-positive breast cancer xenografts

In submission

2. Jun Liu, **Jie Li**, Thomas J Rosol, Xueliang Pan and Jeffrey L Voorhees. Biodegradable Nanoparticles for Targeted Ultrasound Imaging of Breast Cancer Cells in Vitro.

Physics in Medicine and Biology 2007 (52):4739

3. **Jie Li**, Zhongmin Liu, Yunhai Wang, Zaicheng Yu, Mingrong Wang, Qimin Zhan, Zhihua Liu. Allelic imbalance of chromosome 1q in esophageal squamous cell carcinomas from China: a novel region of allelic loss and significant association with differentiation.

Cancer Letters 2005 (220):221

Conference Proceedings

1. Peng-Fei Zhang, **Jie Li**, Jun Liu, Andrew Moiseev, Shizhen Liu, Junghyun Choi, Helene Houle, Mani A. Vannan. Biodegradable polylactic acid nanoparticles for targeted imaging in vitro and in vivo experimental studies.

J Am Soc Echocardiography, 2009, 22(5): 560.

Conference Abstracts

1. **J Li** and J Liu, Targetable nanoparticles for enhanced ultrasound imaging in breast cancer

2009 Annual Fall Meeting of Biomedical Engineering Society (BMES '09), Pittsburgh, PA, October 7-10, 2009.

2. **J Li** and J Liu, Surface Conjugated Nanoparticles for Specific Ultrasonic Enhancement of Breast Cancer Cells.

NanoMedicine Summit 08, Cleveland, OH, USA, September 25-26, 2008.

3. **J Li** and J Liu, Targeted Polystyrene Nanoparticles Affect Ultrasonic Reflectivity of Breast Cancer Cells,

2007 Annual Fall Meeting of Biomedical Engineering Society (BMES '07), Los Angeles, CA, Septembeeer 26-29, 2007.

4. J Liu, **J Li,** A Marcetich, and T Rosol, Herceptin-Conjugated PLA Nanoparticles Targeting Breast Cancer Cells for Ultrasound Imaging.

2006 Annual Meeting of the Society for Molecular Imaging, Hawaii, August 30 - September 2, 2006.

Fields of Study

Major Field: Biomedical Engineering

Table of Contents

Abstract ii

Dedication v

Acknowledgments vi

Vita vii

List of Tables xi

List of Figures xii

Chapter 1: Introduction 1

Chapter 2: Targeted Nanoparticles for Enhanced Ultrasound Imaging of HER2-positive Breast Cancer Xenografts 32

Chapter 3: Biodegradable Polylactic Acid Nanoparticles for Molecular Imaging by Diagnostic Frequency Ultrasound 49

Chapter 4: Multifunctional Polymeric Nanoparticles for Combining Ultrasound Imaging and Drug Delivery in Breast Cancer 62

References 85

List of Tables

Table 1. Polymer repeat unit structure of PGA, PLA, and PLGA 16

Table 2. Physical properties of nongaseous nanoparticle materials 46

Table 3. Particle characterizations of various PLGA nanoparticles 69

Table 4. Stability of fluorescence-loaded PLGA nanoparticles 83

List of Figures

Figure 1. Characteristics of ultrasound contrast agent preparations 5

Figure 2. General targeting outline of ultrasound imaging of ligand-carrying contrast agents retained on a receptor-coated target surface 9

Figure 3. Echocardiography in a canine model demonstrating the presence of a left ventricular thrombus before (left-hand side) and after (right-hand side) intravenous administration of fibrinogen-targeted echogenic immunoliposomes 13

Figure 4. Reaction scheme for the synthesis of PLA-PEG and PLEG-PEG copolymer .. 25

Figure 5. The size distribution of antibody-conjugated PLA nanoparticles 39

Figure 6. SEM images of antibody-conjugated PLA nanoparticles 39

Figure 7. Top: Ultrasound imaging of a MCF-7/HER2-18 tumor xenograft before and after subcutaneous injection of antibody-conjugated PLA nanoparticles. Within 30 minutes post injection, the tumor margins were “enhanced” (arrows in b, c and d). At 1 hour post injection, the tumor was brighter overall. Bottom: Ultrasound imaging of a MCF-7/HER2-18 tumor xenograft before and after subcutaneous injection of PBS. No enhancement was observed. 40

Figure 8. Quantitative analysis of ultrasound enhancement from (a) MCF-7/HER2-18 tumors and (b) MDA-MB-231 tumors, at baseline and post injection with antibody-conjugated nanoparticles or PBS 41

Figure 9. Relative increase of the mean gray scale in MCF-7/HER2-18 tumors at different time points 42

Figure 10. Immunohistochemistry of tumor sections from MCF-7/HER2-18 and MDA-MB-231 xenografts 44

Figure 11. Fluorescent microscope images of SkBr3 cells stained by either Herceptin/nanoparticle bioconjugates or PBS 54

Figure 12. Sonography of livers in gel phantom demonstrating contrast enhancement after the injection of SkBr3 cancer cells treated with antibody-conjugated PLA nanoparticles 55

Figure 13. Relative increase of the mean gray scale of SkBr3 cells treated with PBS (SkBr3 cells + PBS, n=5) or conjugated nanoparticles (SkBr3 cells + NPs, n=6) in mouse livers 56

Figure 14. Top: Ultrasound imaging of a tumor in Her2/neu-overexpressing transgenic mice before and after subcutaneous injection of antibody-conjugated PLA nanoparticles. The contrast enhancement of the tumor could be observed over time compared to baseline. Bottom: Ultrasound imaging of a tumor before and after subcutaneous injection of PBS 57

Figure 15. Quantitative analysis of ultrasound enhancement from tumors at baseline and post injection with antibody-conjugated nanoparticles (n=3) or PBS (n=2) 58

Figure 16. Immunohistology images of Alex Fluor 488 tagged antibody-nanoparticles conjugates (green, B and F) and Hoechst 33342 counterstained nuclei (blue. A and E) of

tumor tissue (C and G) were acquired from tumors treated with antibody-nanoparticle bioconjugates (top panel) and PBS (bottom panel) 59
Figure 17. Dynamic light scattering analysis of PLGA nanoparticles..... 70
Figure 18. Fluorescent microscope images of SkBr3 and MDA-MB-231 cells stained by Herceptin/nanoparticle bioconjugates as samples, and plain PLGA nanoparticles, free fluorescence and PBS as controls 71
Figure 19. Ultrasonic B-mode images of SkBr3 and MDA-MB-231 cells treated by Herceptin/nanoparticle bioconjugates as samples, and plain PLGA nanoparticles, free fluorescence, free antibobody and PBS as controls 72
Figure 20. Comparison of Ultrasound gray scale in SkBr3 and MDA-MB-231 cells..... 74
Figure 21. Time course study of intracellular uptake and retention of PLGA nanoparticles in SkBr3 and MDA-MB-231 cells 76

Chapter 1: Introduction

1. Nanotechnology in medical imaging

Generally nanotechnology deals with structures in nanometer scale, and involves developing materials or devices within that size. It plays an important role in the medical imaging field, for instance, synthesis of nanoparticles as contrast agents via nanotechnology. Contrast agents act as contrast-enhancers because of the high difference of the chemical, physical properties or acoustic impedance mismatch at the interface between the agents and tissue. They are able to significantly improve the quality of the image and help to make a clear diagnosis and guide the medical and surgical management of patients.

1.1. General background of ultrasound contrast agents

Ultrasound contrast agents act as echo-enhancers, because of the high different acoustic impedance at the interface between agent and blood/tissue. The enhanced echo intensity is proportional to the change in acoustical impedance as the sound beam crosses from the blood/tissue to the agent.

Ultrasound contrast agents were studied nearly four decades ago when it was accidentally discovered that air bubbles could be detected in the blood-stream after

injections of agitated aqueous solutions [1, 2]. Since then, slow but considerable progress was made, both in the ability to manufacture ultrasound contrast agents, and in the ability of ultrasound equipment to detect these agents at extremely high sensitivity.

1.2 Properties of ideal ultrasound contrast agent

The ideal ultrasound contrast agent should posses the following set of characteristics [3]:

(1). The agent should be absolutely safe and harmless for the patient. There should be no toxicity for the dose of contrast normally injected. The agent and the products of its decomposition should be completely biodegradable by the body and safely excreted through normal metabolic pathways. No long-term deposition of the agent or its components in the body can be allowed. At the same time, the agent should be stable and robust in vivo and it should stay in the circulation as long as necessary to complete the diagnostic procedures.

(2). The agent should be easily detectable by ultrasound imaging systems and easily distinguished from the tissue background, providing bright contrast to make a clear diagnosis and guide medical and surgical management of the patient. Use of echo contrast agent should also help to monitor the progress of therapeutic interventions and help to avoid other costly diagnostic procedures (e.g., MRI or nuclear medicine examinations).

(3). The amount of contrast agent administered to the patient should be small, preferably in fractions of a milliliter. The administration procedure should be simple (a short intravenous injection is preferred). The agent should require minimal handling and preparation prior to injection.

(4). The contrast material should be stable during storage, preferably, with a shelf life of a couple of years. Room-temperature long-term storage is preferred.

(5). Contrast agent should be inexpensive and easy to manufacture.

1.3 Development of ultrasound contrast agents

So far, the only type of ultrasound contrast agent which has currently been approved by the FDA is shell-stabilized microbubbles [4]. Typically, an ultrasonic contrast agent microbubble contains air or a high-molecular-weigh low-solubility gas encapsulated in a lipid or albumin shell. Sensitivity of the detection of gas-filled microbubbles by ultrasound is quite high, even comparison with other molecular imaging modalities.

However, initial microbubble contrast preparations did not carry a shell and they were quite unstable in the bloodstream [1]. Such shell-free microbubbles could not even pass through the lung vasculature, and contrast imaging of myocardium was only possible after intraarterial administration. Since that time, ultrasound contrast materials' circulation time has improved greatly. Modern microbubble contrasts use appropriate lipid, polymer, or protein shells and these shell-stabilized microbubbles somewhat improve stability over shell-free bubbles.

To improve microbubble stability, we need to prevent direct contact between individual microbubbles and thus reduce the rate of shell fusion and bubble coalescence. This is achieved either by adding electrostatically charged molecules as a part of the microbubble shell [5] or by grafting a surface brush of hydrophilic polymer, such as poly(ethylene glycol) (PEG) on the microbubble surface [3]. PEG brush can prolong circulation time and reduce uptake to macrophage cells in vivo. And PEG coated microbubble preparations even can be stored for up to several years without a substantial loss of ultrasound contrast response.

Gas core is another factor which contributes to circulation time. In the early generation contrast agents, air was used only as the gas phase to improve the backscatter. Now, second generation contrast agent use of low-solubility gases, e.g., decafluorobutane, further improves circulation time, because such gases exit the bubble and dissolve in the surrounding blood slower than oxygen or nitrogen. A lipid monolayercoated bubble with decafluorobutane gas core can stay in the bloodstream for many minutes, up to 1 h for some preparations. This circulation time scale is quite sufficient to perform the task of ultrasound imaging.

For the storage concern, commercially developed microbubbles are usually stored as precursors, mostly dry preparations addition of water for reconstitution prior to injection [5] and can only be used within several hours after reconstitution. However, some of the bubble preparations can withstand prolonged (years) storage in the aqueous phase; this requires a thicker shell, such as denatured albumin or a shell composed of gel-phase lipid combined with PEG brush coating [3] to avoid

microbubble fusion. Overall, storage stability of ultrasound contrast microbubble agents is now comparable with that of other molecular imaging modalities agents, and cumbersome preparation is not required.

Figure 1 shows the characteristics of some microbubble contrast agents [6].

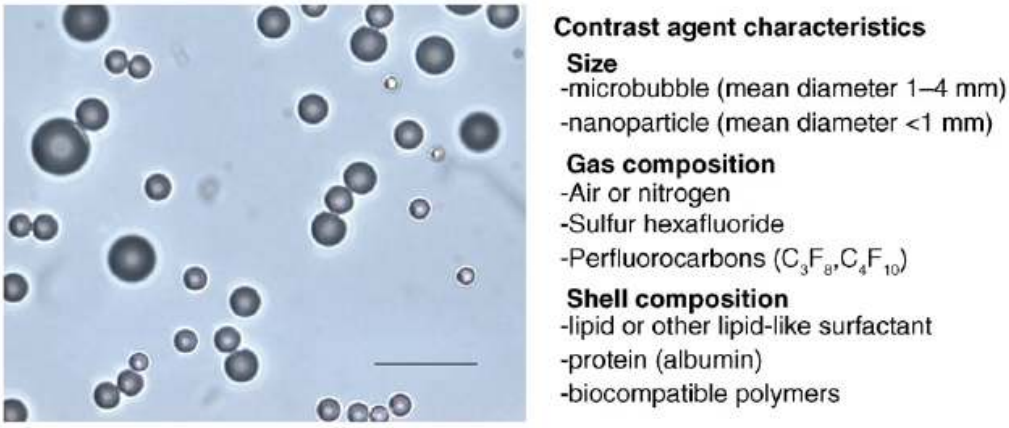

Figure 1. Characteristics of ultrasound contrast agent preparations. The image on the left shows an example of microscopy of a preparation showing typical size distribution (scale bar 10 um). [6]

1.4 Advantages and disadvantages of microbubbles as ultrasound contrast agents

In summary, microbubbles have the following general advantages [3]: 1). Significantly improve the quality of the image and allow easier delineation of the anatomical structures, disease tissues, or tumor metastases. Therefore, it helps making a clear diagnosis and guiding therapy. 2). Only a very small intravenous injection dose is needed for imaging. Typical approved intravenous human dose of ultrasound contrast microbubble material is at sub-milligram level. 3). The

ultrasound contrast agents are manufactured from nontoxic natural or synthetic biodegradable materials, and a small amount of an inert low-solubility non-reactive gas. These components have been shown to be harmless to the patient. 4). The fact that only a small amount of contrast agent is needed for detection makes it possible to consider targeted imaging, where the agent selectively binds to the receptors, for example, on an inflamed endothelium, or marks the diseased tissue. Such agents have not been tested in the clinical trails, but their potentially high sensitivity might allow competition with some radio –pharmaceuticals in the future.

However, microbubbles also have general disadvantages as following [3]: 1). With their size of several microns, they cannot escape from the bloodstream under normal conditions. Thus, the imaging cannot be performed in the areas outside the normal bloodstream. 2). Despite some preparations of microbubbles can persist in the bloodstream for many minutes, majority microbubble agent last only several minutes in the bloodstream. This makes their application less convenient for lengthy multi-plane examinations, and requires multiple administrations or a continuous infusion. 3). Gas-filled microbubble materials are currently approached with caution by physicians, regulatory agencies and industry marketing, despite the fact microbubble-based contrast agents are approved for clinical use in many countries. Because micron-size particulates are seldom used in clinical practice as intravenous agents, especially in diagnostic imaging, a considerable investment and lengthy efforts are required [7]

For the above reasons, ultrasound contrast agents have not yet entered widespread clinical use.

1.5 Other ultrasound contrast agents

Although the ultrasonic contrast agents which are currently in clinical use are generally those based on microbubbles, there is renewed interest in non-gaseous contrast agent [8]. Such as iron particles, perfluorocarbon (PFC), biodegradable nanoparticles and gold-bound colloid microtubules seem to be quite promising [9].

In order to track the fate of transplanted bone marrow-derived cells in the myocardium, Bara et al. labeled the cells with 50 nm iron Dextran beads and then injected them into ischemic hearts of pigs. Transesophageal echocardiography demonstrated the accumulations of labeled stem cells in the myocardium during and 8 weeks after the procedure [10]. Another research group also reported that 24 hours after injection of superparamagnetic iron oxide (SPIO) particles, on the sonogram the gliomas appears inhomogeneously hyperechoic to normal brain tissue with hyperechogic margins in rats [9].

Targeted, liquid PFC nanoparticles have been reported recently that they could provide acoustic contrast enhancement when the agent was bound to a surface layer [11-13]. Unlike those naturally echogenic microbubble formulation, these PFC nanoparticles have poor inherent acoustic reflectivity. However, when a layer effect is induced by collective deposition of nanoparticles occurring on the tissue or cell surface, these nanoparticles generate a local acoustic impedance mismatch that

creates a strong ultrasound signal. Meanwhile, the background signal from unbound, circulating nanoparticles is negligible or absent.

Biodegradable polylactic acid (PLA) nanoparticles with 250 nm mean diameter demonstrated substantial ultrasonic contrast enhancement when they were conjugated with specific ligands and bind to breast cancer cells [14]. By using site-targeting gold-bound microtubules, a stable ultrasound contrast effect could be provided. The contrast intensities of the human thrombi and inflammatory activated human umbilical vein endothelial cells (HUVEC) was significantly increased after their treatment with antifibrin antibody and incubation with gold-bound microtubules and remained high after 20 min of ultrasound exposure.[15, 16] These studies showed the feasibility of using targeted polymeric nanoparticles and gold-bound colloid microtubules to enhance ultrasound images in vitro.

1.6 Targeted imaging with ultrasound contrast agents in general

Targeted imaging is another important development of ultrasound contrast agent. The clinical potential of targeted ultrasonic contrast agent is considerable, both for diagnosis and for drug delivery [8]. The concept of ultrasound contrast agent for targeted imaging consists of using contrast particles with a specific ligand to the target receptors that are expressed in the area of disease. Targeted contrast agent is administered intravenously, circulates in the bloodstream, and accumulates in the area of interest via a ligand-receptor interaction. Targeted agent signal is then used to demarcate the site and condition of the target diseased tissue, and free

circulating agents will be removed by elimination [17]. Therefore, we may expect reduced imaging background and minimized side effect of circulating agents (a simplified picture of such imaging is presented on Figure 2).

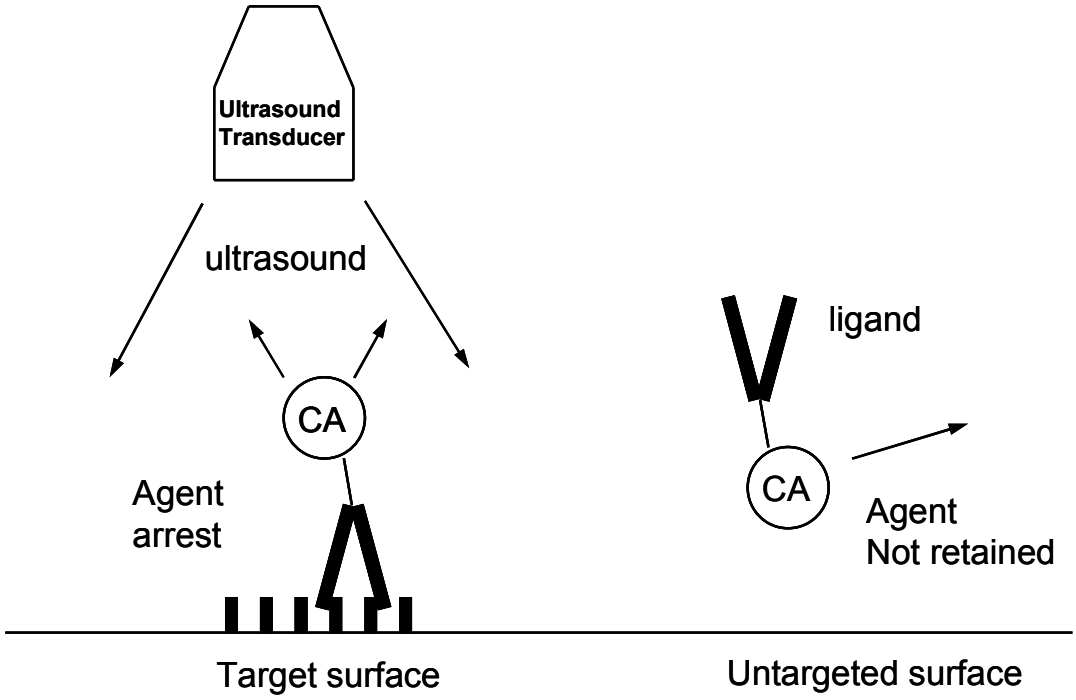

Figure 2. General targeting outline of ultrasound imaging of ligand-carrying contrast agents retained on a receptor-coated target surface. CA: Contrast Agent.

The general targeting strategy consists of attaching disease-specific ligands, such as monoclonal antibodies, glycoproteins, carbohydrates, peptides or peptide mimetics to the contrast agents, either directly or attached to a spacer arm. The use of a flexible polymer spacer arm, for example polyethyleneglycol (PEG) as a linker between the agent surface and the ligand offers some advantage over a direct

attachment. The direct attachment does not offer rapid ligand mobility along the agent surface. Therefore, it may not offer the required time that the matching of ligand and receptor pairs need during the brief contact between the agent and the target surface in a flow-through condition. Use of a flexible polymer tether allows the ligand to rapidly interact with the target surface and attach to the receptors. Additional benefit of placing the ligand on the PEG spacer is that if the ligand is attached directly to the agent surface, it may be hidden inside the polymer brush layer and become poorly accessible to the target receptor [18].

The protein ligand can bind to the contrast agent for covalent or noncovalent attachment. The noncovalent attachment strategies have been well developed, mostly with biotin-streptavidin-mediated techniques [19]. Specifically, after biotinylating the surface polymer through NHS-ester, contrast agents are dispersed in streptavidin solution. After a brief incubation, the excess of free streptavidin is removed by flotation. Biotinylated ligand is then added to complete the “sandwich” formation. Coupling yield for the attachment of biotinylated ligands to agents is reasonably high, and large excesses and losses of expensive ligand can be avoided. However, the streptavidin-biotin coupling technology seems not be suitable for clinically targeted ultrasound contrast agent due to the need of multiple steps and the use of a foreign, possibly immunogenic protein (streptavidin) in the design. That approach is most appropriate and convenient for early proof-of-principle animal studies, where biotinylated ligands, such as antibodies of a wide variety are easily available commercially.

Covalent attachment of antibody ligands to preformed contrast agents can be easily accomplished via certain chemical reactions. For instant, carboxylate is positioned on the polymer surface of agents. Carboxylate can be activated by carbodiimide, such as 1-ethyl-3-(3¢-dimethylaminopropyl) carbodiimide in the presence of *N*-hydroxysulfosuccinimide, and resulting active ester can react with an amino group of an antibody or other protein ligand [7] (Hermanson, 1996) [20]. Another coupling strategy, attachment of thiolcarrying targeting ligands to the particle surface via maleimide [21] or vinyl sulfone, is widely applied in bioconjugate chemistry. Use of maleimide with a formation of a thioether bond, which is exceptionally stable, may provide good ligand coupling yield and slow degradation of the reactive group on the agent surface [7].

For successful targeting between the ultrasound contrast agents and disease-related molecule, the ligands have to be considered. High-affinity small molecular ligands (peptides or peptide mimetics) have some advantages than antibodies. Most of the available monoclonal antibodies are also immunogenic, due to their rat or mouse origin, and the variety of nonimmunogenic human antibodies is still limited. Small molecular ligands are becoming available via combinatorial synthesis and library screening methods. Furthermore, antibodies or other large proteins may be denatured in the harsh conditions of sonication and high shear during preparation. As compared with an antibody, these smaller molecules should easily withstand the conditions of agent preparation without loss of binding affinity. Another advantage of small molecule ligands over antibodies is in the attachment of ligand to receptor.

Antibody active site structure is often designed as a pouch; it binds to the target receptor slowly and holds it firmly. Small ligands, on the other hand, can rapidly bind to the target, which is a great advantage for a situation where a contrast agent that flows through the vasculature and bumps into activated endothelium has a very limited time to attach to it [7, 22].

Overall, the preferred strategy of successful targeting would be to obtain small molecule ligand and attach them to the agents through a covalent linking, preferably via a PEG spacer arm.

Such targeted contrast agents have been tested in animal models (Figure 3), not in the clinical trails yet, but their potentially high sensitivity and specificity might allow the applications in three broad areas: inflammation, angiogenesis, thrombosis [6].

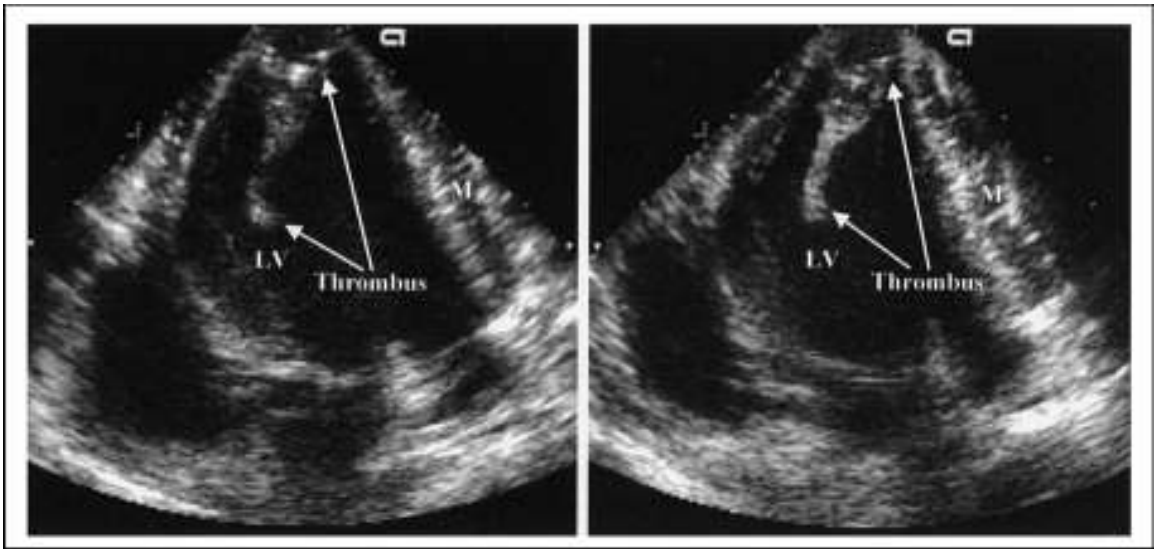

Figure 3. Echocardiography in a canine model demonstrating the presence of a left ventricular thrombus before (left-hand side) and after (right-hand side) intravenous administration of fibrinogen-targeted echogenic immunoliposomes [23].

1.7 Future of contrast ultrasound

Due to proper design of ultrasound contrast agent and new ultrasound imaging technologies and equipment, the quality of imaging will be enhanced and the possibility of undesirable patient side effects will be eliminated with low dosage, improved storage stability, optimal circulation time, reduced nonspecific background accumulation in normal tissues. Ultrasound contrast agents will find widespread application for imaging, image-guided biopsy, and image-guided therapy of cancer.

2. Nanotechnology in drug delivery

Nanotechnology also plays an important role in drug delivery system to transport therapeutics effectively. Delivering of the drug through drug carriers selectively to disease sites and releasing in a controlled rate has been an ultimate goal in drug therapy. Various types of drug carriers, such as virus, liposomes and polymeric nanoparticles, have been developed for the controlled and/or targeted drug delivery. Micro or nanoscale particles can be used as drug delivery vehicles to develop highly selective and effective therapeutic and diagnostic modalities. Nanoparticles have particular advantages in treatment, for example, they can travel through the blood stream without sedimentation or blockage of the microvasculature.

In order to accumulate into the desired sites, in general, targeted nanoparticles comprise the drug, the encapsulating material and the surface coating. The encapsulating material could be made from biodegradable polymers, dendrimers (treelike macromolecules with branching tendrils that reach out from a central core) or liposomes (spherical lipid bilayers). Recently, controlled drug-delivery strategies have made a dramatic impact in medicine. In general, controlled-release polymer systems deliver drugs in the optimum dosage for long periods, thus increasing the efficacy of the drug, maximizing patient compliance and enhancing the ability to use highly toxic, poorly soluble or relatively unstable drugs [24]. Controlled release of drugs (such as small molecules, DNA, RNA or proteins) from the encapsulating material is achieved by the release of encapsulated drugs through surface or bulk erosion, diffusion, or triggered by the external environment, such as changes in pH, light, temperature or by the presence of

analytes such as glucose [25]. Controlled release biodegradable nanoparticles can be made from a wide variety of polymers including poly (lactic acid) (PLA), poly (glycolic acid) (PGA), poly (lactic co-glycolic acid) (PLGA) and polyanhydride. PGA, PLA and their co-polymer PLGA are common biocompatible polymers that are used for making nanoparticles [26]. Since PGA is more susceptible to hydrolysis than PLA, by changing the ratio of these two components, PLGA polymers can be synthesized with various degradation rates.

2.1 PLA/PLGA polymers

Polymer can be nondegradable or degradable. A major disadvantage with nondegradable plymers as imaging agents is that the polymers will need to be removed from the body after the images are acquired. On the contrary, degradable polymers do not require removal and hence are preferred choice in many applications. However, because they degrade to smaller absorbable molecules, it is important to make sure that the resulting monomers are nontoxic.

The most commonly used degradable polymers are Poly (lactic acid) (PLA), Poly (glycolic acid) (PGA) and their copolymer poly(lactide-co-glycolide) (PLGA). These polymers are known to be biodegradable, biocompatible, and nontoxic and have been used for biomedical applications for more than two decades [26]. Poly(l)LA, PGA and PLGA are among the few biodegradable polymers with Food and Drug Administration (FDA) approval for human clinical use. They have been used as sutures, ligament reconstruction, plates and fixtures for fracture fixation devices, vascular grafts, and

scaffolds for cell transplantation [26, 27]. The chemical structures of these polymers are shown in Table 1.

Polymer	Polymer repeat unit structure
Poly(glycolic acid)	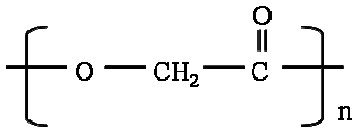
Poly(lactic acid)	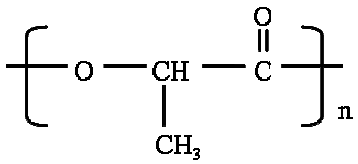
Poly(glycolic-co-lactic acid)	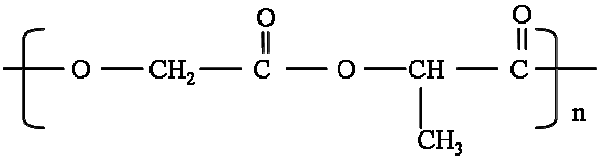

Table 1. Polymer repeat unit structure of PGA, PLA, and PLGA.

Biodegradation of these polymers initially takes place by random hydrolysis of their ester bonds resulting in decrease in molecular weight. This phase is followed by a reduction in mechanical properties, loss of mass and formation of soluble mono and oligomeric products. Finally, natural pathways (metabolism, excretion) harmlessly eliminate the final degradation products. PLA degrades to form lactic acid which is normally present in the body. This acid then enters tricarboxylic acid cycle and is excreted as water and carbondioxide. No significant amounts of accumulation of degradation products of PLA have been reported in any of the vital organs. Carbon[13] labeled PLA has demonstrated little radioactivity in feces or urine indicating that most of

the degradation products are released through respiration. The ultimate fate of glycolic acid in-vivo is considered to be the conversion to carbon dioxide and water, with removal from the body via the respiratory system. PLGA degrades to form lactic acid and glycolic acid, then follows the degrading pathways discussed above [27].

2.2 Strategies of synthesis of PLA/PLGA nanoparticles

Due to their advantages of natural degradation in tissue over a desired period of time, and thus controlled release of encapsulated drugs, over the past decade the utility of biodegradable polymers for pharmaceutical administration has increased dramatically. A number of methods for producing polymeric nanoparticles have been developed, such as emulsion-solvent evaporation, solvent displacement, salting out and spray drying and so on [28].

2.2.1 Solvent Displacement (Nanoprecipitation or Solvent Diffusion) Method

Typically, this method is used for hydrophobic drug entrapment, but it has been adapted for hydrophilic drugs as well. Polymer and drug are dissolved in a polar, water-miscible solvent such as acetone, acetonitrile, ethanol, or methanol [29]. The solution is then slowly transferred (i.e., drop-wise addition) into an aqueous solution with surfactant (e.g. PVA or poloxamer 188) under mild stirring. Nanoparticles are formed instantaneously by rapid diffusion of solvent from the organic phase to the aqueous phase and consequently reduction of interfacial tension and migration of polymer towards the

o/w interface [28]. Finally, the solvent is removed by evaporation under reduced pressure.

The most critical parameters to obtain nanoparticles and avoid bulk polymer precipitation appear to be the polymer concentration and the ratio of organic phase to aqueous phase. And the surfactant may not be necessary for obtaining nanoparticles, but it is important to stabilize and facilitate their redispersion [28].

Solvent displacement method has the following advantages and disadvantages, as compared to other methods:

Advantages:

- The use of non-highly-toxic solvents (i.e., acetone).
- Reduced energy consumption because it only requires regular stirring. The process does not require high stress shear (i.e., sonication or microfluidization).
- Additives can be used for nanoparticle size reduction.

Disadvantages:

- The solvent is removed by evaporation (time consuming).
- The main drawback is the requirement for drugs to be highly soluble in polar solvents (i.e., acetone, ethyl acetate) and slightly soluble in water to minimize losses during solvent diffusion.
- The drug loading efficiency is lower for hydrophilic drugs as compared to hydrophobic drugs because of their poor interaction (hydrophobic interaction) with the polymer leading to diffusion of the drug during the solvent displacement from the polymer in the organic phase to the external aqueous environment.

- Nanoparticle size is very much affected by the polymer concentration; higher nanoparticle sizes are obtained at higher polymer concentrations.

2.2.2 Emulsion Evaporation Method

Emulsion evaporation is the oldest method used to form polymeric nanoparticles from preformed polymers. The method is based on the emulsification of an organic solution of the polymer in an aqueous phase followed by the evaporation of the organic solvent. The polymer is dissolved in a suitable solvent (e.g., ethyl acetate, chloroform, methylene chloride). The organic phase or aqueous phase is poured into the continuous phase (aqueous or organic phase) in which a surfactant (PVA, SDS, Pluronic F68, Span 80) is dissolved to impart stability to the emulsion. Emulsification is carried out under high-shear stress to reduce the size of the emulsion droplet (directly related with the final size of the nanoparticles). The process of emulsification is followed by evaporation of the organic solvent under vacuum, which leads to polymer precipitation and nanoparticle formation. Evaporation under vacuum avoids polymer and active component damage, and promotes final nanoparticle size reduction as well.

Single emulsions, oil in water (o/w) or water in oil (w/o) and double emulsions (w/o/w) can be used to accommodate the entrapment of active components with different properties. The o/w emulsion is used for entrapment of hydrophobic compounds, whereas w/o/w double emulsion is used for the entrapment of hydrophilic compounds. For double emulsion, the water-in-oil-in-water (w/o/w) emulsion formation is sonicated or homogenized for droplet size reduction. This second size reduction should be controlled

to minimize the hydrophilic active component diffusion to the external aqueous phase. This method is widely used for microencapsulation because it is easy to scale-up, it does not require high shear stress and it can be adjusted (by use of the double-emulsion method) to encapsulate water-soluble drugs [29].

The formation of the emulsion is a key aspect of this method, considering that the size of the emulsion droplet is directly related to the final nanoparticle size. Shear stress hence is one of the important parameters to be considered. Other several factors, such as the type and concentration of the polymer and the type and concentration of surfactant, have been shown to affect the characteristics of nanoparticles synthesized by this method. The size of nanoparticles was found to decrease with decreasing polymer concentration in the organic phase and increasing the concentration of the surfactant in the aqueous phase. An increase in the particle size with increasing polymer molecular weight has also been observed [28].

Some advantages and disadvantages of emulsion evaporation are listed below:

Advantages:

- The use of non-highly-toxic solvents (i.e., ethyl acetate).
- Additives can be used for nanoparticle size reduction.
- Suitable for hydrophilic (double emulsions) and hydrophobic active components.

Disadvantage:

- High consumption of energy by the necessity of high stress shear (i.e., sonication or microfluidization).

- The main drawback of the double-emulsion method is the large size of the nanoparticles formed and the leakage of the hydrophilic active component, responsible for low entrapment efficiencies.
- Both the presence of the organic solvent and the application of intense shear forces may cause degradation of labile drugs, such as proteins.

2.2.3 Salting-out Method

In this synthesis method, the polymer is dissolved in a slightly water-miscible solvent, like acetone or tetrahydrofuran (THF). The organic phase is emulsified in an aqueous phase, under vigorous mechanical stirring. The aqueous phase contains the emulsifier and a high concentration of salts which are not soluble in the organic phase. Typically, the salts used are 60% (w/w) of magnesium chloride hexahydrate or magnesium acetate tetrahydrate in a polymer to salt ratio of 1:3. Initially there is no diffusion of the solvent due to the presence of salts. When this o/w emulsion is diluted by fast addition of pure water under mild stirring, the ionic strength is reduced and nanospheres are formed by the migration of the water-soluble organic solvent to the aqueous phase. The final step is purification by cross-flow filtration or centrifugation to remove the salting out agent. Common salting out agents are electrolytes (sodium chloride, magnesium acetate or magnesium chloride) or non-electrolytes, such as ucrose. Important parameters to be considered are: polymer concentration and molecular weight, stirring rate and time, nature and concentration of electrolyte, and stabilizer in the aqueous phase [26, 29].

The salting-out method has the following advantages and disadvantages, as compared to other methods:

Advantages:

- Reduced energy consumption because it only requires normal stirring. The process does not require high stress shear (i.e., sonication or microfluidization).
- Low time-consuming process.
- Suitable for hydrophobic components because the salting out agent is water soluble.

Disadvantage:

- The main drawback is the requirement of a purification step for removal of salting out agent, which is in higher amounts (at least three times more amount of salting out than polymer).

2.2.4 Emulsion Diffusion Method

This method can be considered a modification of the salting out procedure which avoids using salt and thus the need of intensive purification steps. In this synthetic scheme, the polymer is dissolved in partially water-miscible solvent (e.g., benzyl alcohol, propylene carbonate, ethyl acetate) presaturated with water. The organic phase is emulsified with an aqueous solution of a suitable surfactant (i.e., anionic sodium dodecyl sulfate (SDS), non-ionic polyvinyl alcohol (PVA) or cationic didodecyl dimethyl ammonium bromide (DMAB)) under stirring. The equilibrium between the two phases is destabilized by the subsequent addition of water to the system. It causes the diffusion of

the organic solvent and the counter diffusion of water into the emulsion droplets and induces polymer nanoparticle formation [26, 29].

Important parameters that affect the nanoparticle size synthesized by emulsion diffusion are: polymer concentration, solvent nature, surfactant, molecular weight of polymer, viscosity of continuous and discontinuous phase, phase ratios, stirring rate, temperature and flow of water added.

Emulsion diffusion has the following advantages and disadvantages, as compared to other methods:

Advantages:

- The use of non-highly toxic solvents (i.e. benzyl alcohol).
- Reduced energy consumption because it only requires mild stirring. The process does not require high stress shear (i.e. sonication or microfluidization).

Disadvantages:

- The requirement of large amounts of water for nanoparticle formation.
- Large time of emulsion agitation.
- The size is highly sensitive to polymer concentration if the process does not use shear stress for size reduction (high-speed agitation or sonication).

Advantage/disadvantage:

- Suitable for hydrophobic active components. The hydrophilic components have a high migration tendency due to the diffusion of the polar solvent to the aqueous phase and, therefore, the hydrophilic drug entrapment efficiency is low.

2.3 Other techniques related to synthesis of PLA/PLGA nanoparticles

It is generally accepted that PLA and PLGA nanoparticles are rapidly removed from systemic blood circulation following intravenous (i.v.) administration by the macrophages of the mononuclear phagocyte system (MPS) in liver and spleen. The mechanism of nanoparticle recognition by MPS is not specific: Binding of these opsonins onto the surface of NPs, called opsonization, makes them 'visible' to the macrophages [28]. The rapid removal of conventional nanoparticles from the bloodstream limits their potential in controlled drug delivery and targeting. Surface engineering, however, may enhance the capability of nanoparticles to evade MPS uptake, which prolong residence in blood. Hence, it is the key to design long- circulating NPs by surface modification for targeting to the site of disease and successful molecular imaging.

Coating the nanoparticle surface with a hydrophilic polymer such as poly(ethylene glycol) (PEG) has shown some advantages in preventing opsonization and thereby avoiding the MPS uptake [30]. According to the mechanism proposed, surface-grafted chains of flexible and hydrophilic polymers form dense "conformational clouds" preventing other macromolecules from the interaction with the surface even at low concentration of protecting polymer. In contrast, hydrophilic but rigid polymers grafted on the surface of the particle form broad but loose and, thus permeable clouds. Between the hydrophilic polymers, PEG has been found to be a particularly effective steric stabiliser, probably due to its high hydrophilicity, chain flexibility, electrical neutrality and absence of functional groups, which prevent interactions with biological components *in vivo* [28].

The optimum surface density of PEG on nanoparticles plays an important role for the prevention of opsoin deposition. In addition, the length of PEG chains on the surface of nanoparticless is critical to avoid the adsorption of plasma proteins. However, it is considered that surface density has a greater effect than the chain length on low protein adsorption [30].

The PLA-PEG and PLGA-PEG nanoparticles can be synthesized by the methods discussed above from the preformed PLA-PEG or PLGA-PEG copolymers. Diblock PLA-PEG and PLGA-PEG copolymers are synthesised by melt or solution polymerisation of lactide and glycolide in the presence of monomethoxy-poly(ethylene glycol) . The polymerisation takes place in an inert atmosphere. Stannous octoate is the most frequently applied catalyst because it is very effective and has been approved by FDA as a food stabiliser. The reaction scheme and the structures of the copolymers are given in (Figure 4) [28].

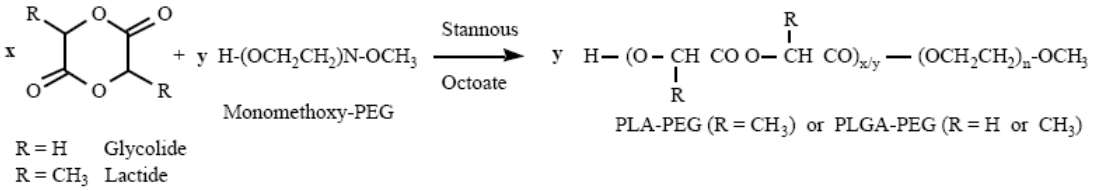

Figure 4. Reaction scheme for the synthesis of PLA-PEG and PLGA-PEG copolymer

One method used for assessing the extent of PEG coating on the surface of pegylated nanoparticles is the measurement of the zeta potential of the aqueous suspension containing nanoparticles. In this method, the mobility of charged particles is

monitored by applying an electrical potential. The zeta potential values may be positive or negative depending upon the nature of the polymer or the material used for surface modification. The extent of surface hydrophilicity can then be predicted from the values of zeta potential [30]. Nanoparticles prepared from PLA-PEG and PLGA-PEG copolymers have low negative zeta potential values (e.g. –6 mV to -4 mV) because the carboxylic acid end groups of PLA/PLGA are capped by the PEG segments [28].

In order to trace the biodistribution of nanoparticles in the body, it is a common strategy to label the nanoparticles by fluorescent dye. Various methods have been reported to prepare the fluorescent nanoparticles: nanoparticles were prepared by the salting-out process with 10% (w/w) of fluorescent-labeled PLA and 90% of unlabeled PLA [31]; nanoparticles were formulated using emulsion solvent evaporation technique and the fluorescent dye was dissolved in the PLGA polymer solution prior to emulsification [32, 33]; and Robert Langer and his colleagues reported that they used the PLA-PEG-COOH nanoparticles and nucleic acid ligands (aptamers) with a 5'-FITC-label and a 3'-NH2 modification to yield fluorescent nanoparticle-aptamer. The acid group on the particle surface was first converted to NHS ester in the presence of EDC and subsequently was covalently coupled to the amine-modified aptamer [22].

2.4 Rapid escape of PLGA nanoparticles into cytoplasm

Cytoplasmic delivery of many macromolecular therapeutics including peptides, proteins, antisense oligodeoxynucleotides (as ODN), and short interfering RNA (siRNA)

remains a significant challenge, because these enzyme-susceptible drugs typically are taken up by targeted cells via endocytosis and trafficked through the endosomal-lysosomal pathway, and thus degradation by lysosomal enzymes and loss of therapeutic activity occurs [34]. Recent studies have shown that PLGA nanoparticles rapidly escape (within 10 minutes) from the endososomal compartment to the cytoplasmic compartment following the intracellular uptake. The mechanism of rapid escape is that the surface charge of nanoparticles reverses from anionic to cationic in the acidic pH of endolysosomal compartment, which leads to the nanoparticles interact with the endo-lysosomal membrane and escape into the cytoplasmic compartment [35]. The rapid escape of PLGA nanoparticles from the degradative environment of the endososomal compartment could protect nanoparticles and the encapsulated therapetutics, resulting in promising sustained release of encapsulated DNA and antiproliferative activity in cancer cells [32, 36].

2.5 Ultrasound promoted nanopartcile-associated drug delivery

Recent research also demonstrates the potential application of ultrasound at diagnostic power levels to promote nanoparticle-associated drug delivery. Besides the fabrication of drug carriers, another barrier existing in drug delivery is sufficient targeting to diseased tissue while limiting deposition elsewhere. It is commonly accepted that attaching a ligand which interacts with a specific surface marker in diseased area will facilitate localized delivery. However, particle vehicles tend to flow along the center of blood vessels and have limited interaction with the targets on the vessel walls [37].

It has been reported that site-specific adhesion efficiency of model drug carriers of latex nanobeads which were loaded on microbubbles can be improved 3~5 folds by localizing microbubbles along a vessel analog (cellulose tube) with ultrasound radiation force (USRF) in shear flow [38].

A method for augmenting drug deposition locally in the tumor cells with the ultrasound generated with conventionally clinical ultrasound imaging equipment has been demonstrated by Crowder's work [39]. In order to direct delivery of selected substances through ultrasound augmented interactions between synthetic nanoparticles and cells, liquid perfluorocarbon (PFC) nanoparticle emulsions were prepared with monolayer lipid-surfactant coats that selectively bind to cell surface receptors via small molecule targeting ligands- antagonist of $\alpha_v\beta_3$-integrin, which can specific target the $\alpha_v\beta_3$-integrin on the human melanoma cells. Ultrasound (mechanical index at 1.9) was applied with a conventional ultrasound imaging system to nanoparticles targeting of $\alpha_v\beta_3$-integrin on human C32 melanoma cancer cells to investigate the influence of ultrasound in nanoparticle-tumor cell targeting. Within 5 min, lipid delivery from nanoparticles into cell cytoplasm was dramatically augmented through the application of ultrasound.

The operation of a potential physical mechanism for this effect could be that the acoustic radiation force on the nanoparticles may contribute to the enhanced lipid delivery. The application of acoustic energy at diagnostic power levels could promote nanoparticle-associated drug delivery by stimulating increased interaction between the nanoparticle's lipid layer and the targeted cell's plasma membrane. The results indicate that local delivery of lipophilic substances (e.g., drugs) from targeted nanoparticles could

be allowed directly into cell cytoplasm and augmented rapidly and safely with conventional ultrasound imaging devices.

Incompressible nanoparticles also experience ultrasound radiation force although that might be smaller compared to compressible microbubbles. It has been reported that in mice models, a dramatic increase in the number of fluorescently labeled polystyrene nanoparticles with a diameter of 100 nm was found in the tumors that were exposed to pulsed high-intensity focused ultrasound [40]. The responses/displacements of soft materials to radiation force may be determined by their mechanical properties, such as stiffness, viscoelastic characteristics, and density; and the local magnitude of radiation force and the generation and propagation of shear waves [41]. It is possible to optimize the response of nanoparticles in the ultrasound field by adjusting the above mentioned parameters, and thus maximize the concentration of drug-loaded nanoparticles on diseased tissue by utilizing ultrasound radiation force.

3. Conclusion

In conclusion, many efforts have been dedicated to develop the nanotechnology in the medical imaging and drug delivery fields, including synthesis of nanoparticles as imaging contrast agents, and/or as drug delivery carriers and promoted nanoparticle-associated drug delivery with conventional ultrasound imaging system.

For biodegradable nanoparticles, the performance of nanoparticles in vivo is influenced by many characteristics, such as particle size, surface chemistry, and hydrophobicity [26]. Hence, appropriate selection of the polymer matrix and

synthesis of nanoparticles in size and mechanical properties are necessary in order to develop a successful ultrasound contrast agent and drug delivery vectors.

Each method available to synthesize PLA/PLGA nanoparticles from preformed polymer has its advantages and disadvantages. The methods based on diffusion of the organic solvent to form the PLGA nanoparticles are limited to low polymer concentration to maintain a nanoparticle mean size of 200 nm. Methods that involve solvent evaporation are more time consuming and expensive, but are less sensitive to changing the polymer concentration. The salting-out method is suitable for formation of nanoparticles at higher polymer concentration, but the involved purification process is a limitation of this synthesis method. However, the principal selection criteria should be the requirements and ultimate application of the nanoparticles.

The nanoparticle size is affected by many parameters. Surfactant concentration, polymer concentration, polymer molecular mass, solvents, and phase ratios play an important role in controlling the size of the nanoparticles in all methods available for nanoparticles formation. It is important to understand the mechanisms involved and manipulate the nanoparticle characteristics by carefully controlling these parameters. Rresearchers are continually attempting to decrease the average nanoparticle size with better control. Some modified techniques have been developed to address the issues of traditional methods, such as membrane emulsion evaporation method, spray dry method, double emulsion with emulsion diffusion and so on [29].

Synthesis of nanoparticles that can perform better in the human body and can modify their responses to special site would be an important future research area, such as

the addition of new polymers to form grafted PLGA [42], surface modification by adding ligands, as well as the creation of nanoparticles with new properties.

The interaction of ultrasound waves with contrast agents allows a drug to be released from the particles selectively at the desired insonified areas of the body, thus allowing targeted delivery of therapeutic agents. Currently, this approach is still far from clinical application. However, the success of such strategies ultimately may reduce systemic side effects because of the use of lower systemic doses of highly effective agents. It is worth considering because it might be a new direction of development of nanotechnology in the ultrasound field, i.e. the conventional ultrasound imaging devices might be used to assist drug conjugated nanoparticles accumulating rapidly and safely into cell cytoplasm.

These pioneering researches provide inspiration for future progress in nanotechnology in the medical imaging and drug delivery fields.

Chapter 2: Targeted Nanoparticles for Enhanced Ultrasound Imaging of HER2-positive Breast Cancer Xenografts

1. Introduction

Breast cancer is one of the most common malignancies in women in the United States. Early detection is important for survival. Ultrasonography has been routinely applied in clinical settings as an adjunct to mammography for breast cancer screening. Currently, its primary role is to differentiate solid tumors from cysts and to guide needle and surgical biopsies [43]. Compared with other medical imaging and diagnostic tools, ultrasound has the advantage of real-time, low cost, and high safety index. However, ultrasound have limited specificity in differentiating tissues with similar acoustical properties [44].

Contrast agents have been developed to introduce exogenous materials with acoustical properties that differ significantly from biological tissue to provide contrast from the tissue of interest. Targeted ultrasound contrast agents will enable enhancement of specific tissue that overexpresses certain biomarkers [6, 12, 45, 46]. We have developed polylactic acid nanoparticles that are surface modified with antibodies to specifically target human breast cancer cells that overexpress the epidermal growth factor receptor-2 (HER2), a well-known tyrosine kinase receptor involved in signal transduction

pathways that regulate epithelial cell growth, differentiation, apoptosis, and metastasis [47]. In a previous report, we demonstrated the specificity and the acoustic enhancement mediated by the PLA nanoparticles in a cell culture model [14].

The objective of the present study is to investigate the feasibility of antibody-conjugated PLA nanoparticles as contrast agents in enhancing the ultrasound images of breast cancer xenografts in a mouse model. Although systemic delivery of the nanoparticle agents is the preferred and envisioned method for their eventual in vivo application, this study focuses on testing the acoustic effects of the particles within the context of intact *in vivo* tumor micro-environment. We have thus opted for a simpler version of the administration of the particles, i.e., localized delivery, to bypass the complications associated with *in vivo* biodistribution. To our best knowledge, this is the first study of testing the ultrasonic contrast enhancement of targeted polymeric nanoparticles in breast tumors.

2. Materials and Methods

2.1. Materials

Polylactic acid (PLA) nanoparticles (Corpuscular Inc., NY) were obtained as 1% (w/v) aqueous suspension, with a mean diameter of 250 nm and surface carboxyl groups (PLA-COOH). 1-ethyl-3-(3-dimethylaminopropyl)-carbodiimide (EDC) was obtained from Polysciences Inc, PA. N-hydroxysuccinimide (NHS), 2-(N-morpholino)-ethane sulphonic acid (MES), and sepharose CL-4B agarose gel filtration medium were obtained from Sigma, MO.

2.2. Particle surface modification

Anti-HER2 monoclonal antibody Herceptin (Genentech, CA) was covalently linked to the PLA nanoparticle surface using a carbodiimide technique as described previously [14]. Briefly, PLA-COOH nanoparticles (0.25 ml, 10 mg mL^{-1}) were suspended in an MES buffer (0.1 M, pH = 5.0), and incubated with 200 μL of 400 mM EDC and 200 μL of 100 mM NHS for 30 min at room temperature with gentle stirring. The activated particles were incubated with Herceptin solution (20 mg/ mL) in 0.5 ml MES buffer (0.1 M, pH = 8.0) for 30 min and the particle suspension was then run through a sepharose CL-4B gel filtration column to remove any remaining unbound antibodies.

After conjugation, the mean diameter and the width of the particle distribution were determined by a dynamic light scattering detector (Nicomp 370, Particle Sizing Systems, Santa Barbara, CA).

The surface morphology and particle size were further confirmed by scanning electron microscopy (SEM). For SEM imaging, drops of nanoparticle suspension were placed on glass coverslips (treated by poly-lysine to increase the adherence of the particles to the coverslip surface). The samples were dried in air overnight at room temperature, and then mounted to metallic stubs, and sputter-coated with gold-palladium. An NOVA nanoSEM (FEI Company, Hillsboro, OR) was used with an acceleration voltage of 5.00 kV to image to nanoparticle samples.

2.3. Cell culture

The MCF-7/HER2-18 cell line, a derivative of MCF-7 breast cancer cells that are stably transfected with a HER2 overexpression vector [48], was used for producing HER2 positive xenografts. The MDA-MB-231 cell line, which has a low expression of HER2 receptors was used as control.

MCF-7/HER2-18 human breast cancer cells were cultured in high glucose DMEM/F12 medium supplemented with 10% heat-inactivated fetal bovine serum (Invitrogen Life Technologies, CA), 1% penicillin-streptomycin, 400 μg/ml Geneticin, G418 (Invitrogen Life Technologies, CA) and 15 μg/ml insulin (Sigma, MO) and incubated at 37˚C in 5% CO_2. MDA-MB-231human breast cancer cells were maintained as previously described [14].

2.4 Human breast cancer xenografts

Human breast cancer xenografts were established in 5- to 7- week-old athymic nude mice (NCI-Frederick Cancer Center, Frederick, MD) by inoculating 5 $\times 10^6$ MCF-7/HER2-18 or MDA-MB-231 cells into the mice subcutaneously on the right flank. The cells were suspended in 100 μl PBS containing 50% matrigel (BD Biosciences, San Jose, CA). Animals were housed in accordance with the Guide for the Care and Use of Laboratory Animals as adopted by the National Institutes of Health. All experiments were carried out in accordance with the animal protocol approved by the Institutional Laboratory Animal Care and Use Committee at the Ohio State University. Institutional guidelines for proper humane use of animals in research were followed.

In the experimental animals inoculated with the estrogen-dependent MCF-7/HER2-18 cell line, 24 hours prior to tumor cell injection and twice weekly thereafter for the duration of the experiment, all mice received subcutaneously 1.5 mg/kg β-estradiol (Sigma-Aldrich, St. Louis, MO) to promote tumor cell growth [49]. Tumors were measured twice-weekly with slide calipers and the volumes (mm^3) were calculated with the formula: 1/2 × major diameter × (minor diameter).^{2} Once tumor volumes reached 150 to 200 mm^3 (typically after 3 weeks of innoculation), the animals were randomly allocated to either the treatment or the control group.

2.5. In vivo ultrasound imaging

Mice (n=12) were anesthetized by isoflurane gas (2-3%), and placed in dorsal position on a heated imaging table (37˚C) under anesthesia. Heart rate and body temperature were monitored during the experimental period. Mice were also warmed by using a supplemental heating lamp.

Mice bearing MCF-7/HER2-18 xenografts (n=6) were divided into two groups, each of which received either (1) 50 µl of Herceptin-conjugated PLA nanoparticles suspended in PBS at 3 mg/ml (n=3); or (2) 50 µl of PBS (n=3). The same procedure was performed on the six mice bearing MDA-MB-231 breast cancer xenografts.

The nanoparticle suspension or PBS was injected subcutaneously close to tumor mass. After injection, a cotton-tipped applicator was used to gently press the needle insertion site to help seal the punctured tissue and prevent leakage. The injection site was

also gently massaged for about ten seconds to assist the distribution of the volume over the tumor mass.

Prior to injections, baseline B-mode images were acquired by using the Vevo 660 high-resolution ultrasound imaging system (VisualSonics Inc., Toronto, Canada). B-mode images were then taken at different time points at 5, 15, 30 minutes, and 1 hour post injection. The system settings for all imaging sessions were identical as follows: power = 100%; gain = 4 dB; TGC = 0 at all locations; RMV scanner = 40B (with a central frequency near 40 MHz). The ultrasound images were acquired at 8- bit amplitude resolution with a pixel gray scale range of 0–255.

A region of interest (ROI) was defined at consistent positions for all B-mode images. The averaged gray scale for each ROI was computed by the image analysis software of the Vevo 660 system.

2.6 Histology

After imaging, the tumors were extracted and fixed in formalin for histological assessment. Routine hematoxylin/eosin staining was performed on formalin-fixed, paraffin-embedded sections (5 μm thick) of tumors. Binding of Herceptin-conjugated PLA nanoparticles on the tumor cells was confirmed by immunohistochemistry. Sectioned paraffin-embedded tumor tissue was deparaffinized in xylene, hydrated in graded concentrations of ethanol (100%, 95%, 75% and 50%) and then hydrated with PBS. The slides were incubated with a solution of fluorescence-tagged antibodies that stain human antibodies (AlexaFluor 488, goat anti-human IgG antibody, Invitrogen, CA)

for 90 min at 1:1000 dilution. Following washing, the slides were incubated with 10 μM Hoechst 33342 (Invitrogen, CA) and mounted for fluorescent microscope imaging. Tissue images were collected using a Zeiss Axiophot (Carl Zeiss Inc, Germany) fluorescent microscope.

2.7 Statistical analysis

Data were expressed as mean ± SD. Difference between and within each group at each time point were analyzed using two-way analysis of variance (ANOVA) test with Turkey-adjustment which employed a mixed model with repeated measurements. A P value < 0.05 was considered statistically significant.

3. Results

3.1 Nanoparticle Characteristics

Herceptin-PLA nanoparticle conjugates were successfully prepared using the carbodiimide technique. The resulting nanoparticles had a mean diameter of 298 nm, with a standard deviation of ± 95.5 nm (Figure 5). The conjugation technique appeared not to significantly alter the particle size. The scanning electron micrograph images of the nanoparticles revealed that the particles maintained regular spherical shape and single suspension after conjugation (Figure 6).

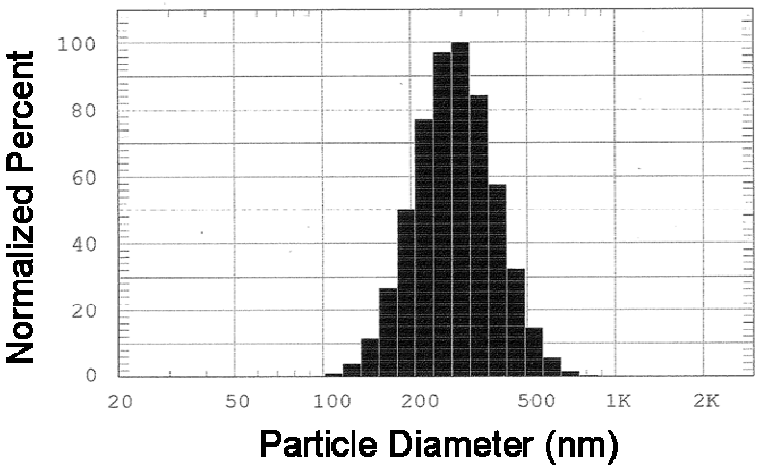

Figure. 5. The size distribution of antibody-conjugated PLA nanoparticles.

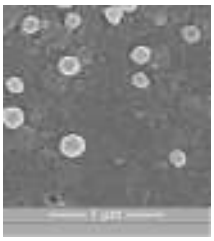

Figure 6. SEM images of antibody-conjugated PLA nanoparticles.

3.2 In vivo ultrasonic enhancement

Examples of ultrasound images in HER-2 positive tumors after treatment with targeted nanoparticles are shown in Figure 7: a-e. The images were obtained at baseline and up to 1 hour post injection. The brightness in the tumor appeared to increase relative to baseline after particle injection. Tumor margin delineation showed enhancement up until 30 min post injection, accompanied by overall enhancement throughout the tumor

over time. Control mice (injected with PBS) did not show changes in the brightness within the tumor over the duration of the imaging period (Figure 7: f-j).

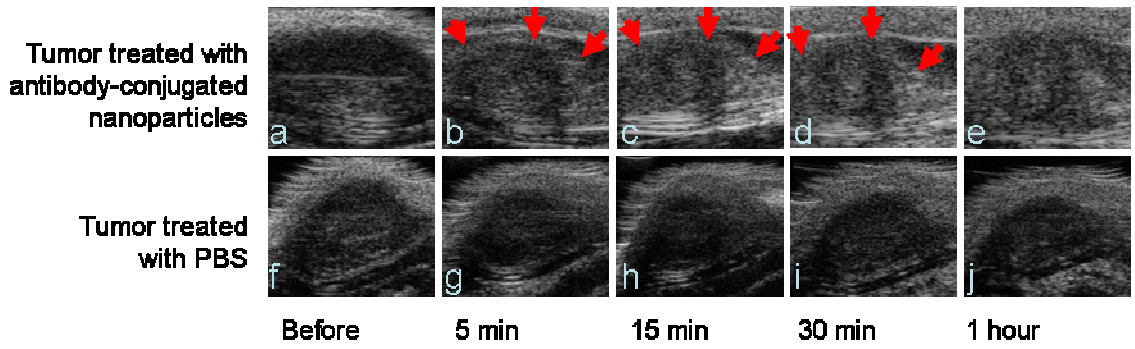

Figure 7. Top: Ultrasound imaging of a MCF-7/HER2-18 tumor xenograft before and after subcutaneous injection of antibody-conjugated PLA nanoparticles. Within 30 minutes post injection, the tumor margins were "enhanced" (arrows in b, c and d). At 1 hour post injection, the tumor was brighter overall. Bottom: Ultrasound imaging of a MCF-7/HER2-18 tumor xenograft before and after subcutaneous injection of PBS. No enhancement was observed.

The average enhancement in contrast intensities of the tumors for each group of mice were shown in Figure 8. The mean grey scale of the ROI was plotted over time. In the treatment group (mice bearing MCF-7/HER2-18 xneograft tumors), the contrast intensity of the tumors significantly increased within 5 min after the treatment with Herceptin-conjugated PLA nanoparticles (69.96 ± 14.72 versus 44.22 ± 3.97, n=3, $p<0.05$; Figure 8a). The signal intensity reached to the maximum value at 15 min (83.14 ± 8.70, n=3), which was significantly different from baseline ($p<0.001$). Although the

brightness of the ROI decreased gradually thereafter, the contrast density remained higher than baseline through 1 hour after the treatment (75.23 ± 9.96 at 30 min, n=3, $p<0.01$ and 61.51 ± 6.54 at 60 min, n=3, $p>0.05$, respectively).

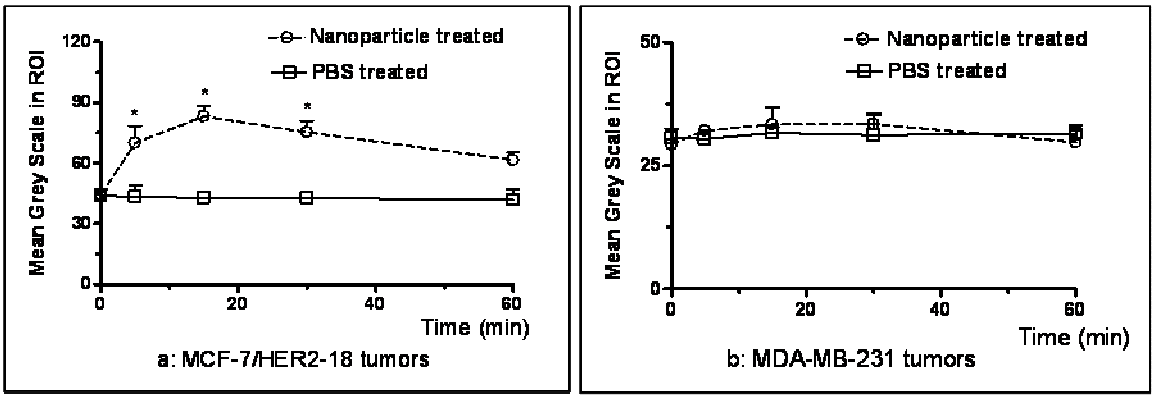

Figure 8. Quantitative analysis of ultrasound enhancement from (a) MCF-7/HER2-18 tumors and (b) MDA-MB-231 tumors, at baseline and post injection with antibody-conjugated nanoparticles or PBS. * $p<0.05$ for comparison between the indicated time and baseline (n=3). Error bars at each point represent standard deviation in three mice.

The corresponding image analysis in the MCF-7/HER2-18 tumors that were treated with PBS showed no change in signal intensities before and after injection (43.86 ± 6.02 at baselines, 42.78 ± 5.56 at 15 min, and 41.87 ± 9.06 at 60 min, $p > 0.05$).

In the control group (mice bearing MDA-MB-231 xneograft tumors), the signal intensity showed no significant enhancement in either nanoparticle-injection group or PBS-injection group (Figure 8b).

In the treatment group (MCF-7/HER2-18 tumors), the comparison between the nanoparticle-injection and the PBS-injection tumors at individual time points was shown in Figure 9. The relative increase of mean gray scale at each time point was calculated as compared to baseline.

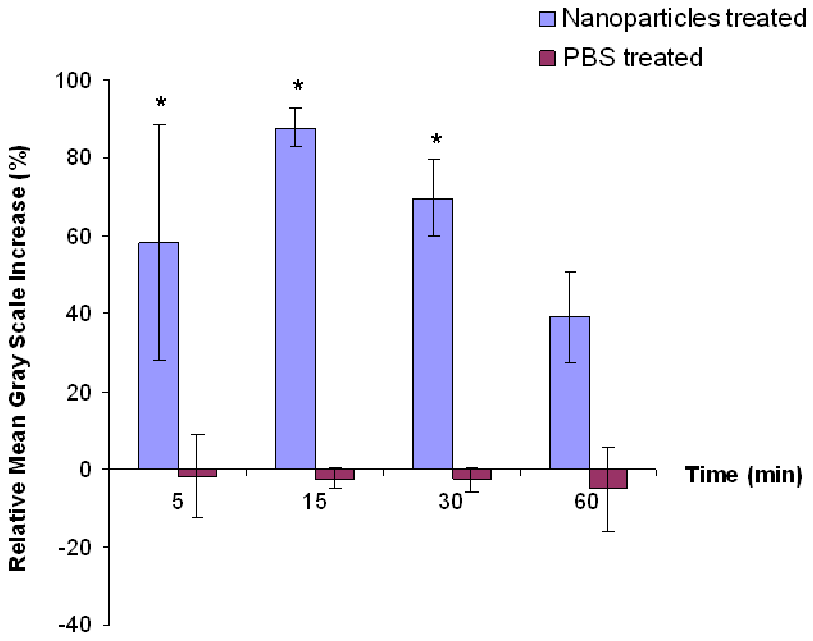

Figure 9. Relative increase of the mean gray scale in MCF-7/HER2-18 tumors at different time points. * $p<0.05$ for comparison between nanoparticle-treated and PBS-treated tumors at the indicated time (n=3).

The average increase of gray scale values for the treatment group with nanoparticle injection were significantly higher than those with PBS-injection at 5 min, 15 min and 30 min (58.32 ± 30.26 % versus -1.94 ± 10.66 %, $p<0.05$; 87.85 ± 4.87 %

versus -2.36 ± 2.65 %, $p<0.001$; and 69.80 ± 9.81 % versus -2.62 ± 3.07, $p<0.01$, respectively). There was no statistical difference in the average increase of gray scale values for MDA-MB-231 xenografts at any time point between the nanoparticle-injection and PBS-injection mice (data not shown).

3.3 Immunofluorescence staining

Fluorescence microscopy confirmed the accumulation of Herceptin-conjugated nanoparticles in HER2 positive tumors (Figure 10a). In the tumors injected with Herceptin-conjugated nanoparticles, significant green fluorescence (Alexa Fluor 488) was observed. The nanoparticles appeared to accumulate in tumor margin (Figure 10b) and more homogeneously distribute in interior area (Figure 10c). PBS injection did not elicit fluorescence signals (Figure 10d).

In contrast, MDA-MB-231 tumors (HER2 negative) did not show relevant fluorescence after either nanoparticle (Figure 10e) or PBS injection.

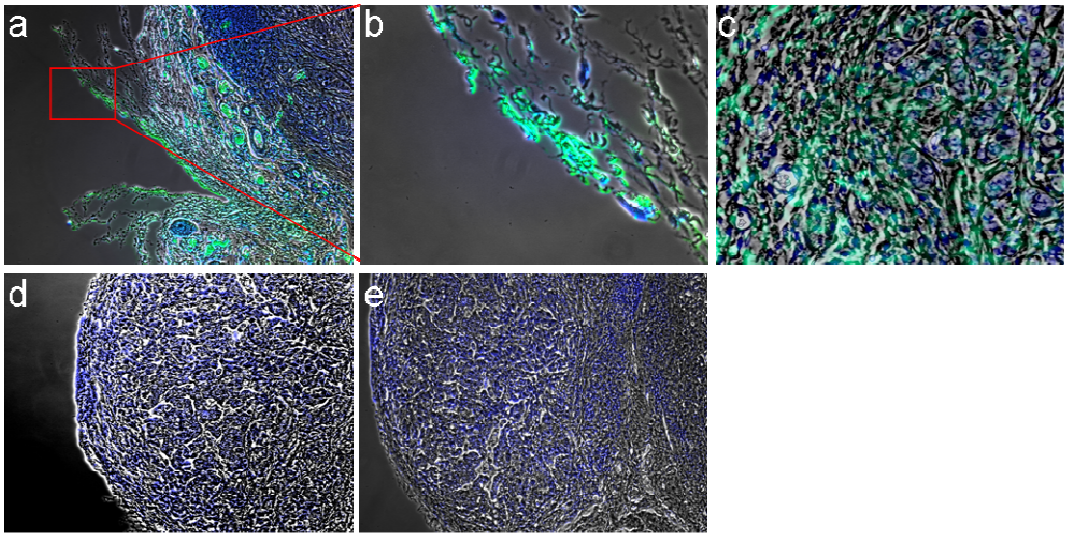

Figure 10. Immunohistochemistry of tumor sections from MCF-7/HER2-18 and MDA-MB-231 xenografts. a: MCF-7/HER2-18 tumor treated with antibody-conjugated nanoparticles. Magnification 10 ×; b: the same region within the red-box in a, but with a magnification of 40 ×. c: MCF-7/HER2-18 tumor (interior area) treated with antibody-conjugated nanoparticles. Magnification 40 ×; d: MCF-7/HER2-18 tumor treated by PBS, 10 ×; e: MDA-MB-231 tumor treated with antibody-conjugated nanoparticles, 10 ×. The nanoparticles were tagged with a green fluorescence (Alexa Fluor 488). Cell nuclei were stained by Hoechst 33342 (blue). Marked green fluorescence was observed in the treatment group (MCF-7/HER2-18 tumors) after injection of antibody-conjugated nanoparticles. No green fluorescence was observed in control group (MDA-MB-231 tumors) under the same imaging settings.

4. Discussion

In the present study, we have demonstrated in a tumor xenograft model the feasibility of targeted PLA nanoparticles for enhancing ultrasound imaging in breast tumor. To our best knowledge, this is the first attempt of using polymeric nanoparticles as targetable ultrasound contrast agents in tumor imaging. Clear delineation of tumor margin was only found in HER2-positive tumor xenografts, but not in tumors that had low expression of HER2 receptors. Injection of PBS into the tumors did not show an acoustical effect. In a control experiment in which a HER-2 positive tumor was treated with non-conjugated particles, no change in the ultrasonic signal intensity was detected before and after particle administration (data not shown). Consistent results were observed in the immunofluorescent staining of the tumor sections, which showed that fluorescence (thus, antibody-conjugated nanoparticles) was only found in HER2 overexpressing tumors. These results suggest that the retention of nanoparticles was site-specific, potentially through receptor-mediated active targeting, and the accumulation of the nanoparticles was responsible for the observed enhancement in sonograms.

Although their natural echogenicity is low, the ligand-directed PLA nanoparticles may have appropriate physicochemical properties to generate acoustic contrast when bound to a surface. It is possible that a local acoustic impedance mismatch was created by these particles when deposited on the surfaces of tissue or cells, inducing a collective contrast enhancing effect [50], similar to the ligand-targeted, lipid encapsulated, nongaseous perfluorocarbon (PFC) nanopaticles. Table 2 shows the calculations of acoustic properties to PLA and two PFC materials considering the bulk material.

Table 2. Physical properties of nongaseous nanoparticle materials.

Material	Density (g/cm^3)	Speed of Sound (m/s)	Acoustic Impedance (x 10^6 kg/s-m^2)	Material/Tissue Impedance Ratio[b]	Reflection Coefficient
PFOB[a]	1.93	632	1.22	0.79	0.11
PBDCO[a]	1.80	680	1.22	0.79	0.11
PLA	1.05	2292	2.34	1.52	0.21

[a]PFOB: Perfluoro-octylbromide; PFDCO: Perfluoro-dichlorooctane [11, 45, 51].

[b]Average tissue properties are assumed as: density = 1.0 g/cm^3, speed of sound = 1540 m/s.

The specific ultrasonic enhancement in HER2-positive tumors appeared within 5 minutes after the injection of the nanoparticles, and the maximum enhancement was achieved at approximately 15 minutes. The signal intensity decreased gradually thereafter, but remained higher than baseline for up to 1 hour. The conjugated nanoparticles likely penetrated the tumor from the periphery to the center of the tumor, resulting in first margin delineation and then throughout enhancement of the tumor. This explanation appeared to be consistent with the results of immunofluorescent staining, in which nanoparticle distribution in both margin and interior region of the tumor was observed. Some agglomerations of particles were observed in the margin of the HER2-positive tumor and more homogeneous distribution of particles was found in the interior region. Additionally, the acoustic intensity of the images appeared to reduce gradually

after 15 minutes post particle-application, which may be associated with the diffusion of the nanoparticles within the tumor and/or endocytosis/elimination of bound nanoparticles by tumor cells. These events may have dampened the acoustic effect of the targeted nanoparticles over time.

There are limitations in the present study. First, PLA was chosen in this study because of its biocompatibility and low toxicity as attested by numerous drug-delivery and tissue-engineering studies [26]. This material may not necessarily provide the optimal acoustic effects. Future studies are needed to test other biocompatible polymeric materials and evaluate their performance as site-targeted ultrasound contrast agents. Secondly, the administration of the particles was not through systemic injection and thus *in vivo* targeting was not examined. Further surface modification (i.e., incorporation of polyethylene glycol) is needed to delay or avoid rapid reticuloendothelial uptake of the particles [28]. Another potential issue to consider is that high frequency ultrasound was used in the present study, while medical imaging systems use much lower frequencies. We acquired images of the study tumors using three transducers at 30 MHz, 40 MHz, and 55 MHz. Consistent contrast enhancement was found within the frequency range tested, indicating that the frequency dependence of the contrast effect was small and may persist at lower frequencies. Future work is needed to confirm the transferability of the findings from this study to medical imaging frequencies.

5. Conclusions

In conclusion, the present study demonstrated significant contrast enhancement using targeted PLA nanoparticles in ultrasonic imaging of HER-2 positive breast cancer xenografts. Although a first step, this study indicated the feasibility of using polymeric nanoparticles to provide specific contrast enhancement for ultrasound imaging of tumors. Nano- or micro- particle systems have drawn increasing interest for targeted diagnostic imaging and drug delivery [14, 16, 52, 53]. Relevant for ultrasound imaging, nanoparticles are stable and relatively insensitive to pressure, heat and shear forces that an imaging agent may experience *in vivo* [12]. The low inherent echogenic properties of nanoparticles may be beneficial to eliminate the background signals from the unbound, circulating contrast agents so they do not interfere with the detection of the bound, targeted agents. Although clinical feasibility is yet to be established, the unique characteristics of nanoparticle agents may bring advantage for their potential use as targeted ultrasound contrast agents.

Chapter 3: Biodegradable Polylactic Acid Nanoparticles for Molecular Imaging by Diagnostic Frequency Ultrasound

1. Introduction

A growing body of literature has substantiated the possibility of molecular imaging via ultrasonography, offering the advantage of real-time, noninvasive visualization of functional, subcellular components or disease-specific epitopes [54]. Contrast agents have been developed, such as microbubbles, echogenic liposome, nanoparticles, etc. with the size ranged from microns to nanos. Nanoparticles have the potential to mimic macromolecules in vivo and can be efficiently surface modified with bio-recognition molecules given their relatively large surface area [14]. By using site-targeting solid nanoparticles, a stable ultrasound contrast effect could be provided [15, 16]. In addition, nanoparticles can extravasate from blood vessel and be uptaken by the targeted cells with higher efficiency compared to microbubbles [55].

Polylactic acid (PLA) is a biodegradable polymer with excellent biocompatibility and biodegradability, and is currently used for surgical sutures, implants and drug delivery devices [56]. In our previous work, a PLA-nanoparticle-based ultrasonic imaging contrast agent for targeted breast cancer markers has been developed and validated with a dedicated small animal ultrasound system (Vevo 660, probe frequency of 40MHz, Visualsonic, Canada). These initial *in vitro* study and *in vivo* animal models are

the first steps towards the eventual goal of clinical application in humans. Because high frequency imaging was used, there may be potential difficulty in translating the results to lower frequencies that are more generally used in medical ultrasound. In this study, we further validated the contrast effect of targeted PLA nanoparticles using diagnostic frequency ultrasound by in vitro and in vivo experimental studies.

2. Materials and Methods

2.1. Materials

Polylactic acid (PLA) nanoparticles (Corpuscular Inc., NY) were obtained as 1% (w/v) aqueous suspension, with a mean diameter of 250 nm and surface carboxyl groups (PLA-COOH). 1-ethyl-3-(3-dimethylaminopropyl)-carbodiimide (EDC) was obtained from Polysciences Inc, PA. N-hydroxysuccinimide (NHS), 2-(N-morpholino)-ethane sulphonic acid (MES), and sepharose CL-4B agarose gel filtration medium were obtained from Sigma, MO.

2.2 Preparation of targeted PLA nanoparticles

Anti-Her2 monoclonal antibody Herceptin (Genentech, CA) was covalently linked to the PLA nanoparticle surface using a carbodiimide technique as reported previously [14].

2.3 Cell cultures

Human breast cancer SkBr3 cells expressing abundant Her2 receptors on the cell membrane were obtained from the American Type Culture Collection (ATCC, VA). The cell cultures were maintained following standard techniques in a humidified atmosphere of 5% CO_2 at 37 degree C with the medium changed every other day.

2.4 Animals

7 BALB/c and 5 Her2/neu-overexpressing transgenic mice were used. The transgenic animal model was developed according to Muller et al. [57] and has spontaneous metastatic disease. Animals were housed in accordance with the Guide for the Care and Use of Laboratory Animals as adopted by the National Institutes of Health. All experiments were carried out in accordance with the animal protocol approved by the Institutional Laboratory Animal Care and Use Committee at the Ohio State University. Institutional guidelines for proper humane use of animals in research were followed.

2.5 In vitro targeting studies

Harvested SkBr3 cells were washed with PBS and incubated with either Herceptin-particle bioconjugates or PBS at room temperature for 30 min, and then further incubated with Alexa Fluor 488 labeled anti-human IgG antibodies (Invitrogen, CA) and counterstained by a nucleus staining agent (DAPI, Vector Laboratories, CA). The targeting of the particles onto cell surfaces was verified by fluorescent microscopy using a Zeiss Axiophot (Carl Zeiss Inc, Germany) fluorescent microscope.

2.6 Ex vivo ultrasound imaging

Seven livers taken from Balb/C mice were washed by PBS and placed into the agarose phantom immersed in a water tank. Suspension (100μl) of nanoparticle-targeted SkBr3 cells was injected through a 26 guage needle into 7 lobes of livers under the monitoring by ultrasonography (Acuson Sequoia 512, Siemens) with a 14 MHz linear probe. The other 5 lobes of livers were injected with the same dosage of PBS suspension of SkBr3 cells only. Images before and after the injection were recorded, and the acoustic intensity within the injection area was analyzed by ImageJ software available from the NIH website. During the injection procedure, the probe was kept steady and the imaging settings including depth, gain, focus and frame rate were kept unchanged. The pixel size and shape of the region of interest (ROI) used in the acoustic intensity analysis was kept the same for images before and after injection.

2.7 In vivo ultrasound imaging

Five Her2/neu-overexpressing transgenic mice were anesthetized by ketamine (20mg/kg) injected intraperitoneally and tape-fixed in dorsal position. Herceptin-PLA bioconjugated nanoparticle suspension (50μl, 2 mg/ml) were injected subcutaneously close to three tumors mass. PBS was injected close to other tumors as control. Ultrasonic images were acquired at baseline and post-injection over time with the orientation and the position of the probe held unchanged with reference to the marker made on the skin. Acoustic intensity within the tumor was analyzed using ImageJ with a circular ROI of 80×80 pixels. Another circular ROI of 10×10 pixels was identified on the skin area above

the tumor and the relative intensity as the value of tumor to that of skin was also calculated.

2.8 Histology

Tumors were harvested and fixed in 4% paraformaldehyde and embedded in paraffin and sectioned at 5 μm thickness. Binding of Herceptin-conjugated PLA nanoparticles on the tumor cells was confirmed by immunohistochemistry. Sectioned paraffin-embedded tumor tissue was deparaffinized in xylene, hydrated in graded concentrations of ethanol (100%, 95%, 75% and 50%) and then hydrated with PBS. The slides were incubated with a solution of fluorescence-tagged antibodies that stain human antibodies (AlexaFluor 488, goat anti-human IgG antibody, Invitrogen, CA) for 90 min at 1:1000 dilution. Following washing, the slides were incubated with 10 μM Hoechst 33342 (Invitrogen, CA) and mounted for confocal microscope imaging (Leica TCS SP2, Leica Microsystems, IL).

2.9 Statistical analysis

Data were expressed as mean ± SD. Difference between and within each group at each time point were analyzed using two-way analysis of variance (ANOVA) test with Turkey-adjustment which employed a mixed model with repeated measurements. A P value < 0.05 was considered statistically significant.

3. Results

3.1 In vitro targeting

The PLA-Herceptin bioconjugates effectively targeting on the Her2 receptors-expressing cells was revealed by the fluorescent microscopy (figure 11). The SkBr3 cells had strong staining by the bioconjugates, but no staining was found in PBS control group.

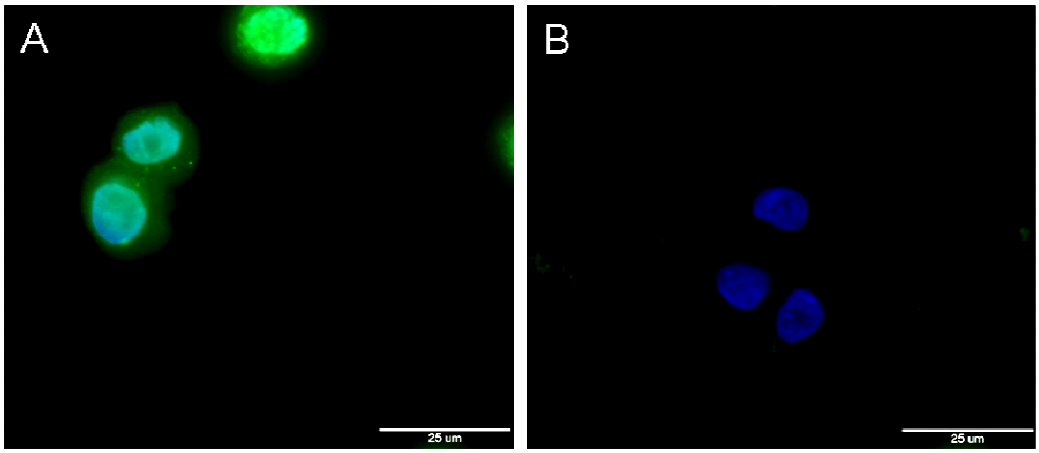

Figure 11. Fluorescent microscope images of SkBr3 cells stained by either Herceptin/nanoparticle bioconjugates or PBS. Herceptin/nanoparticle conjugates were tagged with Alexa Fluor 488 (green). Cell nuclei were counter-stained by DAPI (blue). (A) SkBr3 cells stained by nanoparticle bioconjugates. Substantive staining was found (green) around cell membrane, indicating the abundant binding of bioconjugated nanoparticles on cell membrane. (B) SkBr3 cells treated by PBS and then stained by Alexa Fluor 488 labeled antibodies. No membrane staining was found ruling out the auto-fluorescence.

3.2 Ex vivo ultrasonic enhancement

It has been reported that breast cancer subtypes exhibit distinct patterns of metastatic spread and HER2 expression status were associated with increased risk of spread to specific sites, such as brain, liver, and lung [58]. In this study, an ex vivo experiment where several liver lobes of mice were embedded in agarose gel phantom immersed in a water tank was completed to demonstrate technical feasibility of contrast agent-assisted US assessment of liver metastases. One group of liver tissue was used as the sample where the PLA-Herceptin nanoparticles treated breast cancer cells were injected (figure 12A and 12B). The other group of liver tissue was used as the control where the same amount of PBS treated cells was injected (figure 12C and 12D).

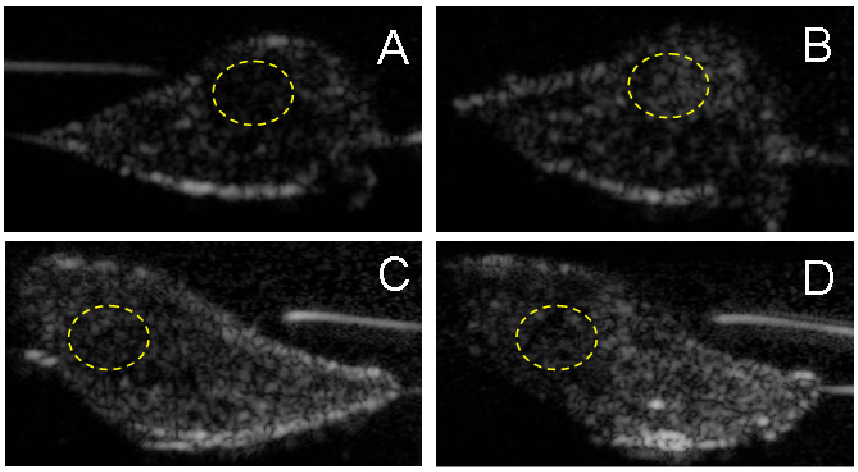

Figure 12. Sonography of livers in gel phantom demonstrating contrast enhancement after the injection of SkBr3 cancer cells treated with antibody-conjugated PLA nanoparticles (B) compared to pre-injection (A). No enhancement was observed in the liver before (C) and after (D) injection of PBS treated SkBr3 cancer cells. Circle shows the injection area.

Enhancement was observed in the area where the injection of nanoparticle-treated SkBr3 cells (figure 12). The acoustic intensity (i.e., gray scale) within this area increased by 84% from 16.0±2.7 to 29.5±6.8 (figure 13). In livers injected with PBS-treated SkBr3 cells, the acoustic intensity remained nearly unchanged from 44.34±13.9 to 38.1±19.7. The slight decrease (-13%) possibly due to the dilution effect of PBS.

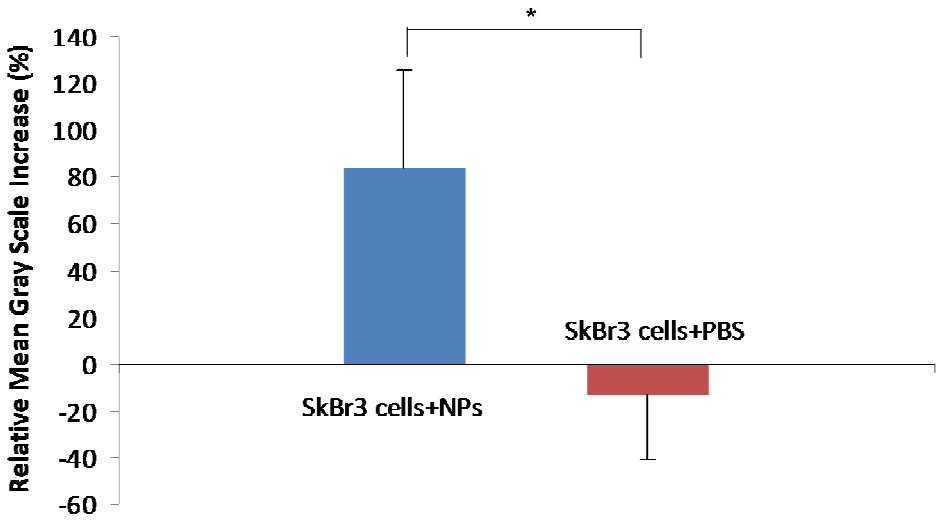

Figure 13. Relative increase of the mean gray scale of SkBr3 cells treated with PBS (SkBr3 cells + PBS, n=5) or conjugated nanoparticles (SkBr3 cells + NPs, n=6) in mouse livers. * $p<0.01$ for comparison between nanoparticle-treated and PBS-treated cells.

3.3 In vivo ultrasonic enhancement

The tumor mass was enhanced by the Herceptin conjugated PLA nanoparticles (figure 14). Both the absolute acoustic intensity within the tumor and the relative intensity increased over time and reached their maximum around 15 minutes respectively after the injection (figure 15). By the end of the experiment at 1 hour, the intensity values were 64.9±20.4, higher than that at baseline (37.5±14.1).

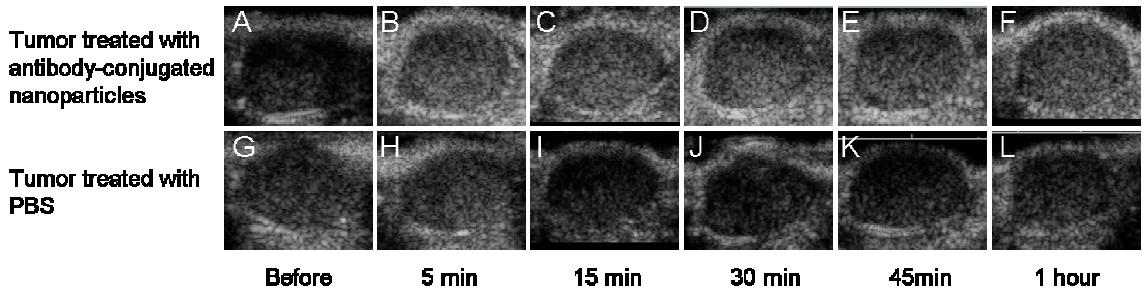

Figure 14. Top: Ultrasound imaging of a tumor in Her2/neu-overexpressing transgenic mice before and after subcutaneous injection of antibody-conjugated PLA nanoparticles. The contrast enhancement of the tumor could be observed over time compared to baseline. Bottom: Ultrasound imaging of a tumor before and after subcutaneous injection of PBS.

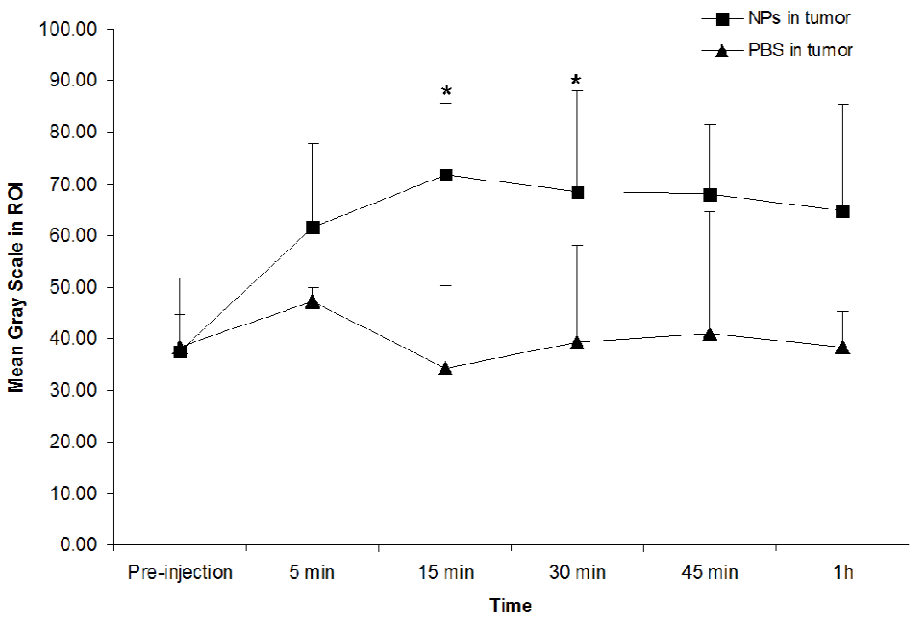

Figure 15. Quantitative analysis of ultrasound enhancement from tumors at baseline and post injection with antibody-conjugated nanoparticles (n=3) or PBS (n=2). * $p<0.05$ for comparison between the nanoparticles treated and PBS treated tumors at indicated time. Error bars at each point represent standard deviation in mice.

3.4 Histology

Confocal microscopy confirmed the hyperechoic regions corresponding to the accumulation of Herceptin-conjugated nanoparticles in tumors (figure 16D). In the tumors injected with Herceptin-conjugated nanoparticles, significant green fluorescence (Alexa Fluor 488) was observed around the tumor cells (figure 16B). PBS injection did not elicit relevant fluorescence signals (figure 16E-H).

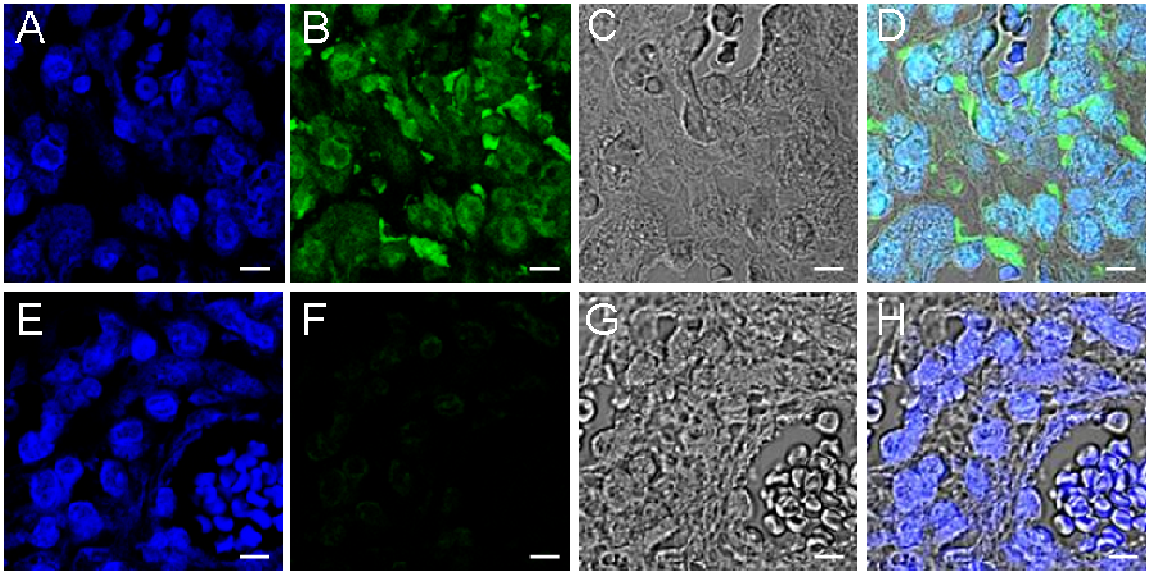

Figure 16. Immunohistology images of Alex Fluor 488 tagged antibody-nanoparticles conjugates (green, B and F) and Hoechst 33342 counterstained nuclei (blue. A and E) of tumor tissue (C and G) were acquired from tumors treated with antibody-nanoparticle bioconjugates (top panel) and PBS (bottom panel). Substantive green staining was found around the cells in tumor with targeted PLA nanoparticles injection (D) while no significant staining was found in tumor with PBS injection as control (H). Bar = 25 μm.

4. Discussion

Nanomolecular imaging is the application of nanobiotechnology in molecular imaging [59]. Nanoparticles may penetrate leaky vasculature or biological barriers of augmented permeability owing to pathophysiological factors and their unique size and reach the target biomarkers in tissue with high efficiency. Thus, nanoparticles hold great values on elucidative imaging from the organism level down to the cellular level which is of importance in diagnosis, therapeutic planning and evaluation.

The PLA polymeric nanoparticles have similar acoustic characterizations to liquid perfluorocarbon particles, which although show poorly echogenic in blood [60] but easily detectable when bound to a surface [61]. Couture et al. [62] developed a sophisticated ultrasonic parameter model to further improve the transmission line model [11, 63] explaining the US reflectivity of submicrometer-sized particles which actively target on a surface. Their study showed that a model which summed the contribution of each scatterer could predict the frequency and confluence fraction dependence of the reflectivity coefficient, and the binding of particles up to a saturation concentration may play an important role in the enhanced reflectivity from a surface. This may explain the contrast effect of targeted nanoparticles observed in the present study - the antibody-PLA bioconjugates accumulated on the cells membrane as shown in the fluorescent microscopy.

Although the polymeric nanoparticles do not possess high echogenicity as microbubbles, in comparison to gas- or lipid-core particles, solid-core nanopartilces like PLA may provide unique advantages especially for in vivo applications as reported before [14, 52], Briefly, PLA nanoparticle has a prolonged imaging time due to its stability in acoustic field; and it has excellent safety and biocompatibility index since PLA is an FDA-approved material for in vivo applications. Besides, these polymeric nanoparticles are surface engineered with biorecognition molecules through covalent binding and there is no need to introduce antibody separately during targeting.

Although the ultrasound imaging resolution in this study was not as high as in our previous study using small animal ultrasound system (Vevo 660), the acoustic intensity

did increase after the injection of targeted PLA nanoparticles in both *ex vivo* and *in vivo* studies (figure 12, figure 13 and figure 14), and reach to the maximum value at 15 min (figure 15), which is quite consistent with the data we obtained from high-resolution ultrasound system. This study has clarified the potential issue of incomparability of the higher frequency (40 MHz) data to lower frequencies (14 MHz) and validated the contrast effect of targeted PLA nanoparticles using diagnostic frequency ultrasound by in vitro and in vivo experimental studies.

The small sample size (only a few transgenic mice were used for the in vivo study) is a limitation of this study. Thus, the results presented are preliminary in nature. Due to the small diameter of PLA nanoparticles and lack of track marker, it is also difficult to directly detect the presence of PLA particles in tissues after the injection. This is another limitation of this study. In future studies fluorescence will be used to track the presence of nanoparticles. Furthermore, the administration of the particles was not through systemic injection and thus *in vivo* targeting was not examined. In order to allow systemic administration, further surface modification (i.e., incorporation of polyethylene glycol) is needed to delay or avoid rapid reticuloendothelial uptake of the particles [28].

5. Conclusion

From our preliminary in vitro and in vivo experimental results, the biodegradable PLA nanoparticles appear to hold great potential as agents for targeted imaging by diagnostic ultrasound.

Chapter 4: Multifunctional Polymeric Nanoparticles for Combining Ultrasound Imaging and Drug Delivery in Breast Cancer

1. Introduction

Nanotechnology emerged in the last few decades brings exciting new possibilities to the field of medicine. It is expected that nanoparticles which can be targeted to a specific tissue or cells to simultaneously detect diseases and deliver therapeutics will lead to more efficacious strategies for detection, diagnosis, and treatment of disease than traditional methods [64, 65].

Efforts have been made to combine microbubble ultrasound imaging agents with drug delivery. Although much progress has been made, the challenge remains for microbubbles to deliver therapeutic levels of drugs or genes at clinically-relevant concentrations. Recent studies showed the efficacy of gene delivery using microbubbles, with a dosage of the microbubble agents much larger (10 to 100 times) than what is recommended for human imaging [66, 67]. Furthermore, tissue damage associated with cavitations, which is typical mechanism for microbubbles to release drugs, could potentially cause safety concerns [68, 69].

Our laboratory has established a biodegradable polymeric nanoparticle platform for enhanced ultrasound imaging. These nanoparticles can specifically target breast

cancer cells through a ligand that is directed to a designated cell membrane marker [14] to generate ultrasound contrast. Based on this platform, specific drug delivery may be simultaneously achieved if the nanoparticles are loaded with therapeutics.

In this study, our purpose is to develop polymeric nanoparticles and evaluate the feasibility of using these nanoparticle agents as a combined platform for ultrasound contrast enhancement and drug delivery. The particle dimensions may play an important role in generating ultrasound contrast as well as overcoming the biological barriers and binding to cells. The secondary goal for this study is to identify an optimal particle size that will result in significant ultrasound contrast enhancement and successful drug delivery.

To our best knowledge, this is the first attempt of using polymeric nanoparticles as dual-mode for ultrasound imaging and drug delivery. Successful development of such a platform may offer great promise for individualized therapy.

2. Materials and Methods:

2.1 Materials

Poly(dl-lactide/glycolide) [50:50] (PLGA) polymer powder (12,000-16,000 Da MW) was obtained from Polysciences (Warrington, PA). Ultrapure deionized water was generated by NANOpure Infinity water purification system (Barnstead International, Dubuque, IA). Rhodamine 6G and Texas Red fluorescence dye was purchased from AnaSpec Inc. (San Jose, CA). 1-ethyl-3-(3-dimethylaminopropyl)-carbodiimide (EDC) was obtained from Polysciences Inc., PA. Poloxamer 188 was obtained from Spectrum

Chemical MFG. Corp., Cardena, CA. N-hydroxysuccinimide (NHS), 2-(N-morpholino)-ethane sulphonic acid (MES), sepharose CL-4B agarose gel filtration medium, acetone and paraformaldehyde were purchased from Sigma–Aldrich (St. Louis, MO). Sodium hydroxide (1.0 N Normal solution) was purchased from Fisher Scientific (Rochester, NY).

2.2 Synthesizing and characterizing PLGA nanoparticles

(1) Synthesis of 150 nm PLGA Nanoparticles (denoted as "PLGA-NP $_{150}$"): PLGA nanoparticles were prepared by using modified solvent displacement method. Briefly, 7.5 mg of PLGA polymer powder was dissolved in 2.5 ml acetone completely. This PLGA solution was added drop-wise into 5 ml of 0.25% poloxamer/PBS solution. The emulsion was allowed to stir 5 min at 40 °C and 500 rpm with a 2cm magnetic stirrer. The mixture was then homogenized at 90W for 2 min using an Omni Ruptor 250 ultrasonic probe (Omni International, Waterbury, CT). After evaporation of the solvent using rotary evaporator (Yamato RE500) for 30 min, the nanoparticles were collected and redispersed in PBS.

(2) Synthesis of 300 nm PLGA Nanoparticles (denoted as "PLGA-NP $_{300}$"): PLGA-NP $_{300}$ were prepared similarly as PLGA-NP $_{150}$, except that 12.5 mg of PLGA polymer powder was dissolved in 2.5 ml acetone completely. The probe sonication was not needed.

(3) Synthesis of 500 nm PLGA Nanoparticles (denoted as "PLGA-NP $_{500}$"): PLGA-NP $_{500}$ were prepared similarly as PLGA-NP $_{300}$, except that 25 mg of PLGA

polymer powder was dissolved in 2.5 ml acetone completely, and then was added drop-wise into 2.5 ml of 0.25% poloxmer/PBS solution.

For fluorescent microscopy, 40 uM of Rhodamine G6 fluorescent dye was dissolved in the PLGA polymer solution prior to mixture with aqueous phase. And for confocal microscopy, 40 uM of Texas red dye solution was added to the organic solution prior to emulsification.

After synthesis, the mean diameter and the width of the particle distribution were determined by a dynamic light scattering detector (BI 200SM, Brookhaven Instruments Corporation, Worcestershire, NY). All particle size data refer to volume-weighted distributions. The zeta potentials (ζ) of PLGA nanoparticles were determined in PBS on a ZetaPALS instrument (Brookhaven Instruments Corp., Worcestershire, NY).

To determine the concentration of particles in different size, the mass of particles in volume unit (ml) was weighed after frozen-dry by LYPH LOCK 4.5 (Labconco Corporation, Kansas City, MO). The same concentration of the particles (mass/ volume) was used to compare their capabilities as ultrasound contrast agents and drug delivery vehicles.

2.3 Conjugating PLGA nanoparticles with Heceptin

Anti-HER2 monoclonal antibody Herceptin (Genentech, CA) was covalently linked to the PLGA nanoparticle surface using a carbodiimide technique as described previously[14]. Briefly, PLGA nanoparticles (0.25 ml, 3 mg mL^{-1}) were suspended in an MES buffer (0.1 M, pH = 5.0), and incubated with 200 μL of 400 mM EDC and 200 μL

of 100 mM NHS for 30 min at room temperature with gentle stirring. The activated particles were incubated with Herceptin solution (20 mg/ mL) in 0.5 ml MES buffer (0.1 M, pH = 8.0) for 30 min and the particle suspension was then run through a sepharose CL-4B gel filtration column to remove any remaining unbound antibodies.

2.4 Cell culture

Human breast cancer cell lines SkBr3 and MDA-MB-231 were obtained from the American Type Culture Collection (ATCC, VA). The cells were cultured in Dulbecco's modified Eagle medium (DMEM) supplemented with 10% fetal bovine serum (FBS), 1% L-glutamine and 1% penicillin streptomycin (Invitrogen Life Technologies, CA). The cell cultures were maintained in a humidified atmosphere of 5% CO_2 at 37^0C with the medium changed every other day.

2.5 Targeted binding of PLGA nanoparticles and cancer cells

In this study, SkBr3, a human breast cancer cell line expressing abundant HER2 receptors on the cell membrane, was used as the positive cell line and MDA-MB-231, another breast cancer cell line, has a low expression of Her2, as the negative cell line for testing receptor-mediated specificity of nanoparticle targeting.

Confluent monolayers of SkBr3 or MDA-MB-231 cells were detached with trypsin/EDTA and dissociated into cell suspensions. SkBr3 and MDA-MB-231 cell samples were treated with excessive nanoparticles (2 mg/mL) to achieve saturated binding. Individual samples of the cells were washed with PBS and incubated with

Herceptin-PLGA nanoparticle bioconjugates, same dose of plain PLGA nanoparticles, free fluorescence dye in PBS, free antibody in PBS, and PBS control at room temperature for 30 min. After incubation, the cells were washed with PBS, fixed in 4% paraformaldehyde, and imaged ultrasonically.

Fluorescent microscopy was performed to verify the targeting of the particles onto cells. The Rodamine G6 encapsulated in the nanoparticles was used as fluorescent marker to identify the presence of nanoparticles.

2.6 In vitro ultrasound imaging

To simulate the targeting of the particles onto a tissue surface, a layer of cells with different treatment was deposited on agarose gels (2–4%) with the same area. And then these cell layers were imaged by a Vevo 660 high-resolution ultrasound imaging system (VisualSonics Inc., Toronto, Canada). The system settings for all imaging sessions were identical: power = 100%; gain = 14 dB; TGC = 0 at all locations; RMV scanner = 40B (with a central frequency near 40 MHz). The acoustic pressures (in water) under this imaging setting are P+ = 7.21 MPa, and P− = −7.53 MPa. B-mode images were acquired at 8 bit amplitude resolution with a pixel gray scale range of 0–255.

A region of interest (ROI) was defined at consistent positions for all frame images. The averaged gray scale for each ROI was computed by the image analysis software of the Vevo 660 system. Two sample t-tests were performed to analyze the difference of the average gray scale for particle-targeted cells and control cells.

2.7 In vitro drug delivery studies

Human breast cancer cells were seeded at a cell density of 50 000 cells/ml on coverslips in 24-well culture plates and grow to confluence in an incubator prior to the experiment. The cells were randomly divided into 4 groups: conjugated-NP, plain NP, free-fluo and PBS treated group. In conjugated-NP group, the cells were incubated with 200 μl of conjugated PLGA nanopartilces (2 mg/ml) loaded with fluorescent dye for 30 minutes, and the medium was removed and replaced by fresh cell culture medium. For plain-NP group, plain nanopartilces of equivalent dose was added to a separate group of cells. In free-fluo and PBS groups, cells treated with free fluorescence (40 μM) and PBS respectively were used as controls to account for autofluorescence.

The medium was changed on the second day following treatment and on every alternate day thereafter through 7 days. On each day, one coverslip was randomly selected and thoroughly rinsed with PBS to remove medium and then fixed with 4% paraformaldehyde. The coverslips were examined by using a confocal microscope (Nikon Eclipse Ti, Nikon Inc., Melville, NY,) to evaluate the drug delivery efficiency of nanoparticles by observation of the intracellular localization of the nanoparticles in cells [32, 70].

2.8 Statistical analysis

Data were expressed as mean ± SD. Difference between and within each group at each time point were analyzed using two-way analysis of variance (ANOVA) test with Turkey-adjustment which employed a mixed model with repeated measurements. A P value < 0.05 was considered statistically significant.

3. Results

3.1 Nanoparticle Characterization

The mean size, the zeta potential and polydispersity of various PLGA nanoparticles determined by dynamic light scattering (DLS) are presented in Table 3. At pH 7.4, the PLGA nanoparticles prepared in this study showed negative zeta potential, in agreement with the results reported by other researchers [71]. The polydispersity indexes are very small (less than or approximately to 0.1), indicating narrow size distribution [72]. Figure 17 shows the DLS analysis of the mean size distribution of the PLGA nanoparticles.

Table 3. Characterizations of PLGA nanoparticles.

PLGA nanoparticle preparations	Mean particle size (nm)	Zeta potential ± S.D. (mV)	Polydispersity index
PLGA-NP $_{150}$	152.5	-17.47±2.16	0.143
PLGA-NP $_{300}$	300.9	-59.22±1.91	0.018
PLGA-NP $_{500}$	499.5	- 55.39±-0.78	0.035

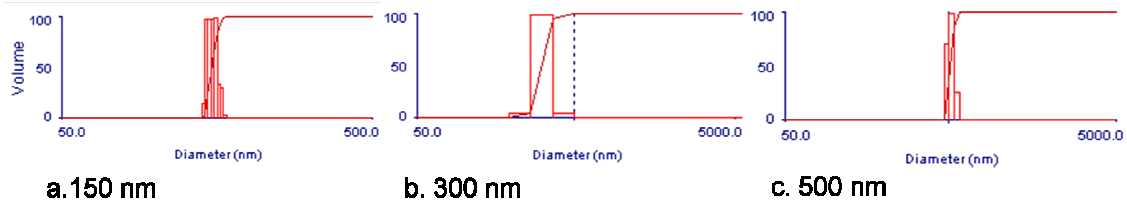

Figure 17. Dynamic light scattering analysis of PLGA nanoparticles. Mean size distribution of (a) 152.5 nm; (b) 300.9 nm; and (c) 499.5 nm.

3.2 Targeted binding of PLGA nanoparticles and cancer cells

Fluorescent microscopy shows strong staining in SkBr3 cells after treatment with nanoparticle–Herceptin bioconjugates of different sizes (150, 300 and 500 nm) (Figure 18). MDA-MB-231 cells were negative for nanoparticle–Herceptin bioconjugates staining, demonstrating the receptor-mediated specificity of PLGA nanoparticle targeting (Figure 18). Furthermore, no staining was found in plain nanoparticles, free fluorescence or PBS treated SkBr3 and MDA-MB-231 cells (Figure 18), ruling out the non-specific binding or autofluorescence from the background.

The Skbr3 cells treated with nanoparticle–Herceptin bioconjugates of 500 nm showed higher fluorescence intensity compared to bioconjugates of 150 nm and 300 nm (Figure 18). Considering the less volume of the smaller size particles at the same surface area, it may be due to that PLGA-NP $_{150}$ and PLGA-NP $_{300}$ show much lower encapsulation efficiencies of fluorescence dye than PLGA-NP $_{500}$ [73]. And the deposited layer of nanoparticles on cell membrane is thinner than PLGA-NP $_{500}$ under saturated binding.

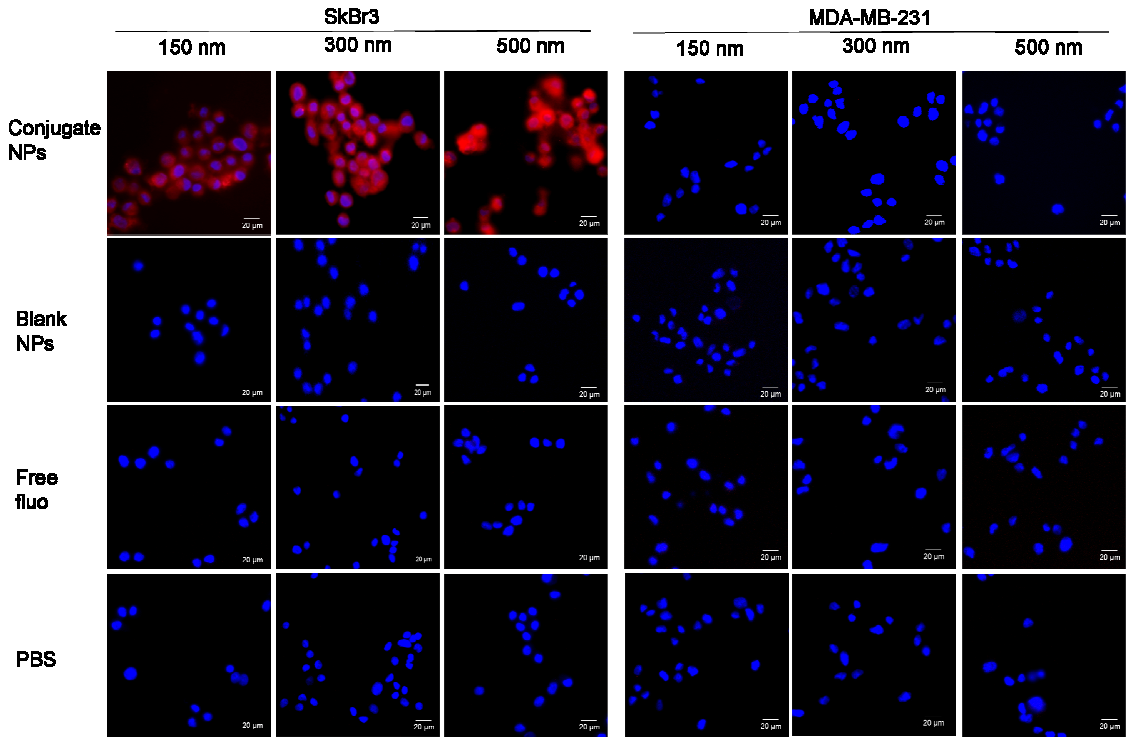

Figure 18. Fluorescent microscope images of SkBr3 and MDA-MB-231 cells treated by Herceptin/nanoparticle bioconjugates, plain PLGA nanoparticles, free fluorescence and PBS. Both Herceptin/nanoparticle conjugates and plain nanoparticles were encapsulated with Rodamine G6 (red). Cell nuclei were counter-stained by DAPI (blue). Substantive red staining was found in SkBr3 cells after treatment with nanoparticle bioconjugates of all three sizes (150, 300 and 500 nm). No staining was found in MDA-MB-231 cells after treatment with nanoparticle bioconjugates. No staining was found in samples treated with plain PLGA nanoparticles, free fluorescence and PBS. Bar = 20 µm.

3.3 In vitro ultrasound imaging

SkBr3 cells treated with 300 nm and 500nm conjugated nanoparticle appeared significantly brighter in ultrasound B-mode images than the control groups including

those treated with the same dose of plain nanoparticles, free fluorescence, free antibody and PBS (Figure 19). The 150nm particles increased cell echogenicity but the increase did not achieve statistical significance. The nanoparticle-targeted SkBr3 cell layer appeared hyperdense compared to the cells without nanoparticle targeting. This echogenicity was not found in MDA-MB-231 cells regardless of the treatment.

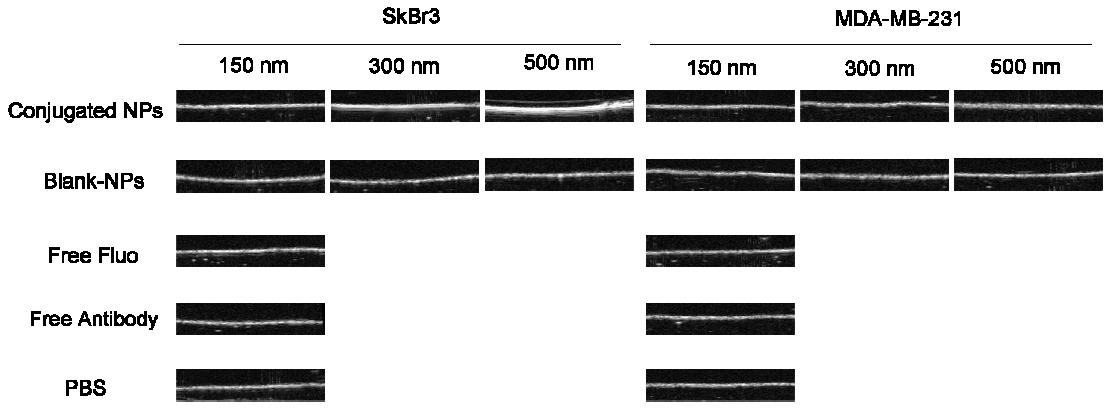

Figure 19. Ultrasonic B-mode images of SkBr3 and MDA-MB-231 cells treated by Herceptin/nanoparticle bioconjugates, plain PLGA nanoparticles, free fluorescence, free antibobody and PBS. All samples contained the same number and concentration of cells. SkBr3 cells with Herceptin/nanoparticle bioconjugates treatment (300 nm and 500 nm) demonstrated significantly enhanced echogenicity.

The brightness of the images was quantified by the average gray scale value of the ROIs defined on the B-mode images. The average gray scale values for 300 nm and 500 nm nanoparticle-targeted SkBr3 cells were significantly higher than those of the plain nanoparticle treated (non-targeting) SkBr3 cells (173 ± 6 in bioconjugates treated cells

versus 131 ±7 in plain particles treated cells for 300 nm size, and 184 ± 13 in bioconjugates treated cells versus 131 ±7 in plain particles treated cells for 500 nm size, respectively; $n = 5$, $P < 0.001$, Figure 20). They were also significantly higher than those of free fluorescence, free antibody and PBS treated SkBr3 cells ($n = 5$, $P < 0.001$, Figure 20).

The average gray scale value of 150 nm bioconjugated nanoparticle-targeted SkBr3 cells did not show significant difference from those of control groups and was significantly lower than those of 300 nm and 500 nm nanoparticle-targeted SkBr3 cells (145 ± 6 in 150 nm bioconjugates treated cells versus 173 ± 6 in for 300 nm, and 184 ± 13 in 500 nm, respectively; $n = 5$, $P < 0.001$, Figure 20)

There was no statistical difference in the average gray scale for MDA-MB-231 cells between the nanoparticle-treated and control groups (Figure 20).

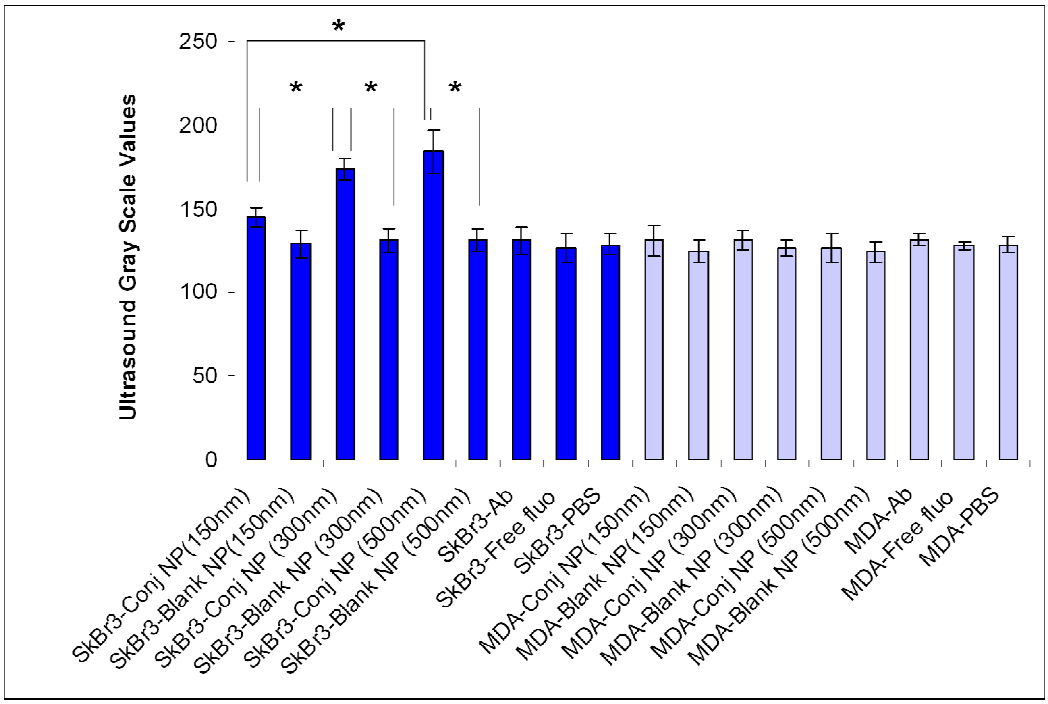

Figure 20. Comparison of Ultrasound gray scale in SkBr3 and MDA-MB-231 cells. Data are presented as mean ± standard deviation, n=5; * $p < 0.01$. The ultrasonic gray scale values of the SkBr3 cells increased significantly after treatment with the Herceptin-conjugated nanoparticles of 300nm and 500 nm size. This enhancement was not detected in MDA-MB-231 cells that had a low expression of the surface receptors.

3.4 In vitro drug delivery studies

SkBr3 cells treated with antibody-conjugated PLGA nanoparticles of all three sizes (150 nm, 300 nm and 500nm) demonstrated the red fluorescence of nanoparticles (due to Texas Red incorporated in nanoparticles) mainly within 1 day (Figure 21). At day 1, cells treated with 150 nm bioconjugates showed a significantly greater amount of nanoparticles intracellular localized in the cells than those treated with 300 nm

bioconjugates. Over time, the fluorescence gradually decreased in SkBr3 cells treated with either 150 nm or 300 nm conjugated nanoparticles. The fluorescence was detectable until day 4 in the 150 nm group whereas the level of fluorescence reduced dramatically on day 3 and disappeared on day 4 in the 300 nm group.

For SkBr3 cells treated with 500 nm conjugated nanoparticles, the red fluorescence was mainly present around the cells indicating that the majority of nanoparticles accumulated on the cell membrane, instead of intracellular localization (Figure 21).

The SkBr3 cells treated with plain nanoparticles, and the MDA-MB-231 cells treated with conjugated nanoparticles and plain particles of various sizes did not exhibit fluorescence at any time point post-treatment, except for a few random non-specific precipitations of nanoparticles (Figure 21). It suggests that the association of the conjugated nanoparticles with cells may be achieved via the receptor-mediated specific targeting of PLGA nanoparticle.

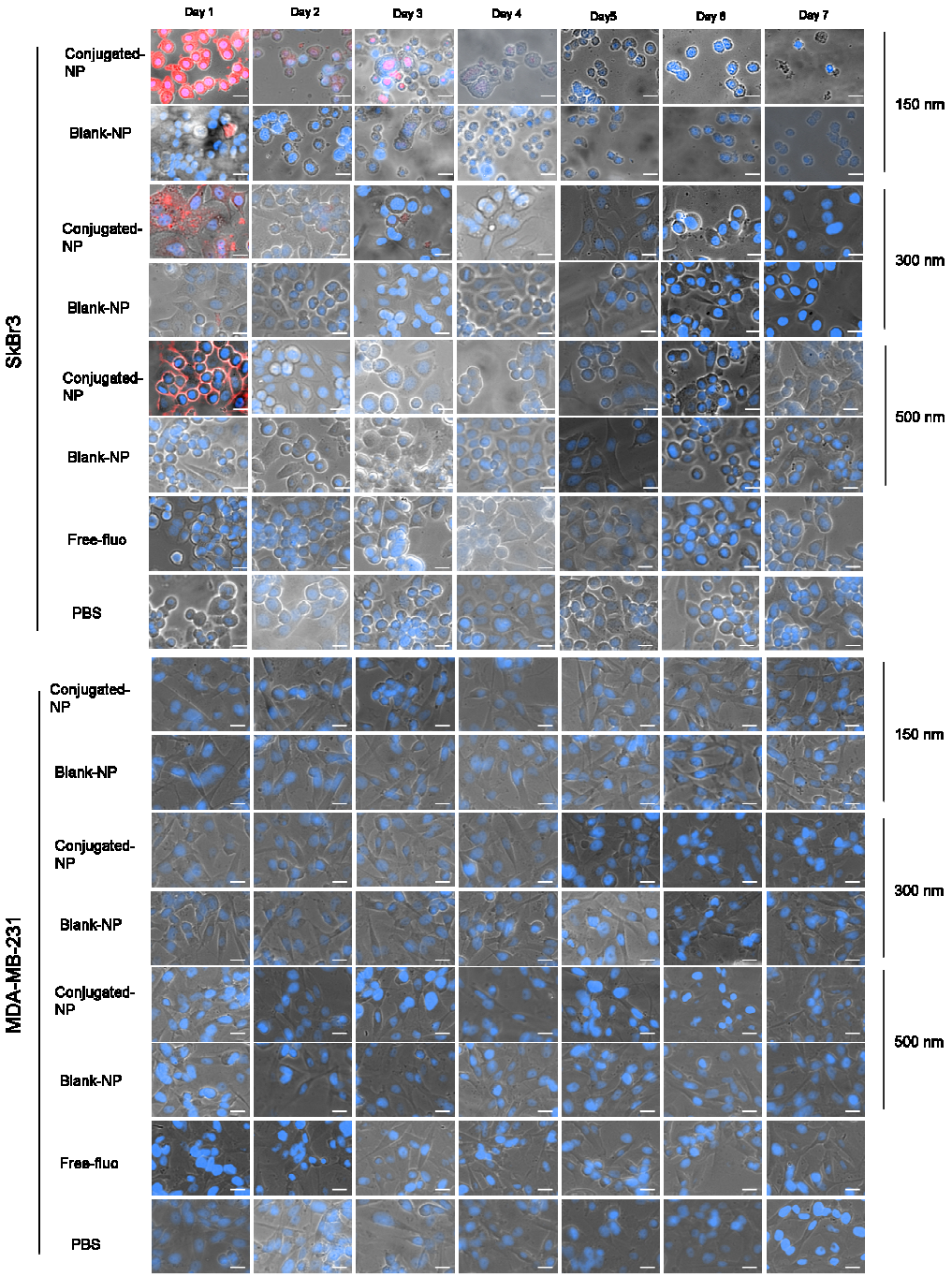

Figure 21. Time course of uptake and retention of PLGA nanoparticles in SkBr3 and MDA-MB-231 cells. Cells were treated with Herceptin-bioconjugated nanoparticles or plain nanoparticles. The PLGA nanoparticles were incorporated with Taxes Red (red

fluorescence). Cells incubated with free dye or PBS were used as controls. Cell nuclei were counter-stained by DAPI (blue). SkBr3 cells treated with bioconjugated nanoparticles at 150 nm or 300 nm demonstrated sustained particle localization as opposed to transient membrane accumulation in the cells treated with 500 nm bioconjugates.

4. Discussion

Breast cancer is one of the most common malignancies among women in the United States [75].In order to provide very specific information about cellular structure and function to help diagnose and treat cancers, various imaging modalities are used in clinic today. Ultrasonic imaging (sonography) is now routinely applied in a clinical setting as an adjunct to mammography in breast cancer screening. Its role is primarily to differentiate solid tumors from cysts and to guide needle and surgical excision biopsies [43]. Ultrasound provides real-time 2-D or 3-D imaging at relatively low cost. It is also safe for repeated application to monitor of therapeutic outcome over time.

The progression of breast cancer from in situ hyperplasia to metastatic disease involves interplay among cellular genetics and microenvironmental factors; the former can be monitored using molecular imaging and the later using other ultrasonic methods [43]. Most molecular imaging approaches include development of blood-born particles with biologically active surfaces. These particles, known as imaging contrast agents, target disease-specific molecular sites in the body and emit or reflect energy that can be sensed by current imaging modalities [76-78]. Development of such agents is helpful to

increase the diagnostic information provided by ultrasound scans so that the number of questionable biopsies of patients at risk can be reduced with progressing diagnostic performance, which also can be used regularly for monitoring a patient's response to treatment.

Multifunctional imaging contrast agents that combine diagnostics and treatment of diseases have recently gained more and more interests. The potential dual use of nanoparticles for both imaging and site targeted delivery of therapeutic agents offers great promise for individualizing therapeutics. 1) Based on imaging, these multifunctional nanoparticles could enable conclusive assurance that the drug is reaching the intended target. 2) The drug delivery nanoparticles that are available with noninvasive imaging techniques offers a tool for rapid, noninvasive, serial follow-up monitoring of treatment response. Synergistically combining targeted drug delivery and molecular imaging, detection and quantification of these nanoparticles at the targeted site may ultimately give instant verification of delivery plus confirmation of therapeutic efficacy through serial characterization of the specific molecular epitope expression. 3) For targeted therapeutic agents, the mechanisms of drug delivery become more complicated than traditional medicines. For instant, the serum concentrations are not necessarily indicative of the amount of drug accessible to the desired site. And by targeting the carrier to the tissue of interest, the drug is locally released to that area, resulting in a much higher effective drug concentration at the site than is indicated by serum levels alone. The ability to quantify the local concentrations of these particles could be of great

benefit for estimating local drug concentrations and developing new pharmacokinetic and pharmacodynamic paradigms to describe this new class of agents [53, 79].

Traditional ultrasound imaging contrast --microbubbles have been reported to be used as drug delivery vehicles [80]. However, as a drug reservoir, the lipid-monolayer shelled microbubbles were restricted to specific drug types and had limited loading capacity [81]. Instead of gas-core microbubbles, polymeric nanoparticles are promising candidates for multifunctional carriers integrated contrast agents with drug delivery. One important biomedical application of biodegradable polymers is controlled drug delivery, which has been reported by many researchers [33, 72, 82].And the contrast enhancing effect of targeted polymeric nanoparticles for ultrasound imaging has been demonstrated in our previous studies [14].

In this study, we aim to develop multifunctional polymeric nanopaticles with the desired dimensional and surface properties which can be used as drug delivery vehicles and ultrasound contrast agents, and assess if the fabricated nanoparticles have sufficient capability to be a combined platform for enhanced ultrasound imaging and drug delivery by using *in vitro* phantoms. PLGA nanoparticles were simultaneously loaded with therapeutic agents (fluorescence marker) to generate a targeted imaging/delivery agent that can be monitored by ultrasound. And the testing of the functionality of the particles as image-enhancing agents, as well as delivery vehicles in *in vitro* phantoms was completed. The contrast-enhancing capability of the engineered nanoparticles was tested using a high-resolution ultrasound imaging system to examine whether they can be tracked by sonography based on their unique acoustic properties. The ability of

nanoparticle in drug delivery was examined by observing the localized delivery of therapeutic agent into cells via confocal microscopy.

Successful synthesis of nanoparticles is a fundamental problem in this work. The ideal nano-carrier need to satisfy many criteria, such as nano-scale uniform size, convenient operation, the flexibility to be functionalized with surface targeting ligands, specific binding on target tissue, the ability to encapsulate fragile cargos, effective enhancement of imaging contrast and so on. Many efforts have been made to develop synthesis methods for nanoparticles that meet these criteria. However, conventional methods for nanoparticles synthesis usually require elaborate operations and strict reaction conditions and result in size distribution that leans toward micron scale instead of nano scale. In order to address the above issues of conventional methods, several methods have been developed recently to synthesize PLA or PLGA nanoparticles from the pre-formed polymers [28]. The strategy used in present study to prepare nanoparticles produced desired characterizations of PLGA nanoparticlesare. Through adjusting the reaction conditions and the concentrations of polymer and surfactant, a series of PLGA nanoparticles was created with desired mean size and low polydispersity (table 3 and Figure 17). After conjugation with anti-HER2 antibodies, all these particles (PLGA-NP $_{150}$, PLGA-NP $_{300}$ and PLGA-NP $_{500}$) demonstrated effective targeting on SkBr3 cells which express abundant HER2 receptors (figure 18). Consistently, the enhanced ultrasonic appearance was only found in SkBr3 cells treated with antibody-conjugated nanoparticles, not in SkBr3 cells treated with plain nanoparticles which lack of anti-HER2 antibodies or in MDA-MB-231 cells that have low expression of HER2 receptors,

suggesting that the targeted nanoparticles contributed to the observed ultrasonic enhancement (Figure 19).

It is interesting to note that echogenicity of SkBr3 cells increased along the size augmentation of targeted nanoparticles according to the quantitative determination of average gray scale value of the B-mode images (Figure 20). However, the PLGA-NP $_{150}$ did not demonstrate statistical significance between the bioconjugated nanoparticle treated SkBr3 cells and plain nanoparticle treated cells, or other control SkBr3 groups (free antibody, free fluorescence and PBS treated), which was opposite to the results of PLGA-NP $_{300}$ and PLGA-NP $_{500}$. It suggests that the particle size may be the effectors of the reflected acoustic power. Generally polymeric particles with larger size will have stronger back-scattered power [83]. Previous study in our lab demonstrated consistent results in polystyrene particles [52]. However, there was no statistical significance between PLGA-NP $_{300}$ and PLGA-NP $_{500}$ bioconjugates targeted SkBr3 cells. This could be because that the echogenicity enhancement generated by PLGA-NP $_{300}$ has reached the saturation that can be detected by B-mode imaging, especially when the saturation binding of nanoparticles may form a layer on cell surface[63] .

The Texas-Red fluorescence marker incorporated in the nanoparticles (dissolved in the polymer phase) appeared to be stably associated with the polymer matrix of nanoparticles during the experimental time frame in the present study. In order to investigate the stability of fluorescence loaded PLGA NPs during the experimental time frame, Herceptin conjugated PLGA-NP$_{150}$, PLGA-NP$_{300}$ and PLGA-NP$_{500}$ nanoparticles (2 mg/ml) were prepared, and three aliquots (0.25 ml) of each preparation were obtained.

The fluorescent intensity and the dry mass of the particle samples were measured at three time points: A1: immediately after preparation, A2: after incubation in cell culture medium for four days, and A3: after incubation in cell culture medium for five days. The A2 and A3 particle samples were incubated in 0.5 ml of cell culture medium in a humidified atmosphere of 5% CO_2 at 37^0C. Prior to measurements fluorescence intensity and dry mass, the nanoparticles were centrifuged and resuspended in PBS. The fluorescence intensity was measured by using an USB4000-FL fluorescence spectrometer (Ocean Optics Inc., Dunedin, FL) at the excitation wavelength of 590 nm and the emission wavelength of 618 nm. The particle suspensions were lyophilized and the dry mass was weighed by an analytical balance (M-220, Denver Instrument Inc., Bohemia, NY). The fluorescence intensity and the mass of the particle samples measured at the three time points were compared (Table 4). Minimal decrease of fluorescence intensity (approximately 12% decrease compared to initial intensity) was observed, likely in association with nanoparticle degradation (11%~14% decrease in particle mass as compared to initial values, Table 4). The fluorescent dye incorporated in nanoparticles appears to be sensitive and stable markers for evaluating the cellular uptake of nanoparticles by confocal microscopy [74].

The fluorescence gradually decreased over time in SkBr3 cells treated with either 150 nm or 300 nm conjugated nanoparticles (Figure 21). This may be caused by the combined effect of the particle degradation in cells [32] and exocytosis of nanoparticles. The nanoparticle concentration in the extracellular medium was low (except during the incubation of the cells with the particles). Thus, after the particles were uptaken by the

cells, the cycling of endocytosis and exocytosis could be altered, resulting in a decrease in intracellular nanoparticle level [70]. The red fluorescence was detectable until a few days after the single treatment of conjugated PLGA-NP_{150} and PLGA-NP_{300}, suggesting the intracellular retention and possible sustained release of loaded drug in these two groups.

Table 4. Stability of fluorescence-loaded PLGA nanoparticles

PLGA nanoparticles	Initial		Day 4		Day 5	
	Fluorescence Intensity (a.u.)	Mass (mg)	Fluorescence Intensity (a.u.)	Mass (mg)	Fluorescence Intensity (a.u.)	Mass (mg)
PLGA-NP $_{150}$	48009	0.5	44076	0.47	42405	0.43
PLGA-NP $_{300}$	47940	0.5	49811	0.5	41889	0.43
PLGA-NP $_{500}$	47448	0.53	48176	0.53	41638	0.47

In this study, only the SkBr3 cells treated with PLGA-NP $_{150}$ and PLGA-NP $_{300}$ bioconjugates demonstrated significant and sustained intracellular localization of nanoparticles (Figure 21), suggesting that the endocytosis uptake of nanoparticles by the cells following the receptor-mediated specifically targeting. Interestingly, no significant uptake was observed in the SkBr3 cells treated with PLGA-NP $_{500}$ bioconjugates, a possible reason for the above phenomenon could be the fact that the naoparticles of 150 nm and 300nm undergo receptor-mediated endocytic uptake process whereas the 500nm is size cut-off described for phagocytosis [70, 84].

Summarizing all results described above, in order to create ideal multifunctional polymeric nanoparticles for combining ultrasound imaging and drug delivery, optimization will require compromise among size, echo-genicity and drug delivery. Therefore, PLGA-NP $_{300}$ is most likely to be the promising candidate because it has both capabilities of significant contrast enhancement and specific drug delivery on cancer cells.

5. Conclusion

To be successful at this research, a truly interdisciplinary effort involving nano-fabrication, surface chemistry, imaging, and drug delivery is required. A novel polymeric ultrasound contrast agent-based drug delivery vehicles has been developed in this study. Compared to the other two sizes (150 nm and 500nm), particles at middle size (300nm) have more suitable combination of contrast enhancement and drug delivery to act as powerful US scatterers and effective therapeutics carriers. Ultrasound imaging contrast of cancer cells can be significantly enhanced by targeting of these polymeric nanoparticles, meanwhile the loaded therapeutic agents in the naoparticles can be specifically delivered into cancer cells. This work will improve the ability to monitor treatment outcome and the efficacy of targeted drug delivery using ultrasound, which is a safe, cost-effective, and readily available imaging and therapeutic modality.

References

1. Gramiak, R., P.M. Shah, and D.H. Kramer, *Ultrasound cardiography: contrast studies in anatomy and function.* Radiology, 1969. **92**(5): p. 939-48.
2. Kremkau, F.W., et al., *Ultrasonic detection of cavitation at catheter tips.* Am J Roentgenol Radium Ther Nucl Med, 1970. **110**(1): p. 177-83.
3. Klibanov, A.L., et al., *Detection of individual microbubbles of an ultrasound contrast agent: fundamental and pulse inversion imaging.* Acad Radiol, 2002. **9 Suppl 2**: p. S279-81.
4. de Jong, N., et al., *Principles and recent developments in ultrasound contrast agents.* Ultrasonics, 1991. **29**(4): p. 324-30.
5. Bokor, D., et al., *Clinical safety of SonoVue, a new contrast agent for ultrasound imaging, in healthy volunteers and in patients with chronic obstructive pulmonary disease.* Invest Radiol, 2001. **36**(2): p. 104-9.
6. Kaufmann, B.A. and J.R. Lindner, *Molecular imaging with targeted contrast ultrasound.* Curr Opin Biotechnol, 2007. **18**(1): p. 11-6.
7. Klibanov, A.L., *Ligand-carrying gas-filled microbubbles: ultrasound contrast agents for targeted molecular imaging.* Bioconjug Chem, 2005. **16**(1): p. 9-17.
8. Wells, P.N., *Ultrasound imaging.* Phys Med Biol, 2006. **51**(13): p. R83-98.
9. Nolte, I., et al., *Iron particles enhance visualization of experimental gliomas with high-resolution sonography.* AJNR Am J Neuroradiol, 2005. **26**(6): p. 1469-74.
10. Bara, C., et al., *In vivo echocardiographic imaging of transplanted human adult stem cells in the myocardium labeled with clinically applicable CliniMACS nanoparticles.* J Am Soc Echocardiogr, 2006. **19**(5): p. 563-8.
11. Hall, C.S., et al., *Experimental determination of phase velocity of perfluorocarbons: applications to targeted contrast agents.* IEEE Trans Ultrason Ferroelectr Freq Control, 2000. **47**(1): p. 75-84.
12. Hughes, M., et al., *Perfluorocarbon nanoparticles for molecular imaging and targeted therapeutics.* Proceedings of the IEEE, 2008. **96**(3): p. 397-415.
13. Marsh, J.N., et al., *Molecular imaging with targeted perfluorocarbon nanoparticles: quantification of the concentration dependence of contrast enhancement for binding to sparse cellular epitopes.* Ultrasound Med Biol, 2007. **33**(6): p. 950-8.
14. Liu, J., et al., *Biodegradable nanoparticles for targeted ultrasound imaging of breast cancer cells in vitro.* Physics in Medicine and Biology, 2007. **52**(16): p. 4739-4747.

15. Bekeredjian, R., et al., *Potential of gold-bound microtubules as a new ultrasound contrast agent.* Ultrasound Med Biol, 2002. **28**(5): p. 691-5.
16. Korosoglou, G., et al., *The potential of a new stable ultrasound contrast agent for site-specific targeting. An in vitro experiment.* Ultrasound Med Biol, 2006. **32**(10): p. 1473-8.
17. Schneider, M., *Characteristics of SonoVuetrade mark.* Echocardiography, 1999. **16**(7, Pt 2): p. 743-746.
18. Kim, H.J., et al., *Possibility of wound dressing using poly(L-leucine)/poly(ethylene glycol)/poly(L-leucine) triblock copolymer.* Biomaterials, 2000. **21**(2): p. 131-41.
19. Lindner, J.R., et al., *Ultrasound assessment of inflammation and renal tissue injury with microbubbles targeted to P-selectin.* Circulation, 2001. **104**(17): p. 2107-12.
20. Bogdanov, A.A., Jr., A.L. Klibanov, and V.P. Torchilin, *Protein immobilization on the surface of liposomes via carbodiimide activation in the presence of N-hydroxysulfosuccinimide.* FEBS Lett, 1988. **231**(2): p. 381-4.
21. Kirpotin, D., et al., *Sterically stabilized anti-HER2 immunoliposomes: design and targeting to human breast cancer cells in vitro.* Biochemistry, 1997. **36**(1): p. 66-75.
22. Farokhzad, O.C., *Nanoparticle-aptamer bioconjugates: a new approach for targeting prostate cancer cells.* Cancer research, 2004. **64**(21): p. 7668.
23. Hamilton, A., et al., *Left ventricular thrombus enhancement after intravenous injection of echogenic immunoliposomes: studies in a new experimental model.* Circulation, 2002. **105**(23): p. 2772-8.
24. Siddhartha, S., *Nanofabrication for drug delivery and tissue engineering.* Digest Journal of Nanomaterials and Biostructures, 2008. **3**(4): p. 257-263.
25. Langer, R. and D.A. Tirrell, *Designing materials for biology and medicine.* Nature (London), 2004. **428**(6982): p. 487.
26. Bala, I., S. Hariharan, and M. Kumar, *PLGA nanoparticles in drug delivery: The state of the art.* Critical reviews in therapeutic drug carrier systems, 2004. **21**(5): p. 387-422.
27. Gunatillake, P.A. and R. Adhikari, *Biodegradable synthetic polymers for tissue engineering.* European cells & materials, 2003. **5**: p. 1-16; discussion 16.
28. Avgoustakis, K., *Pegylated Poly(Lactide) and Poly(Lactide-Co-Glycolide) Nanoparticles: Preparation, Properties and Possible Applications in Drug Delivery.* Current Drug Delivery, 2004. **1**(4): p. 321-333.
29. Astete, C. and C. Sabliov, *Synthesis and characterization of PLGA nanoparticles.* JOURNAL OF BIOMATERIALS SCIENCE-POLYMER EDITION, 2006. **17**(3): p. 247-289.
30. Soppimath, K., et al., *Biodegradable polymeric nanoparticles as drug delivery devices.* Journal of Controlled Release, 2001. **70**(1-2): p. 1-20.
31. Nobs, L., et al., *Biodegradable Nanoparticles for Direct or Two-Step Tumor Immunotargeting.* Bioconjugate chemistry, 2006. **17**(1): p. 139-145.

32. Prabha, S. and V. Labhasetwar, *Nanoparticle-mediated wild-type p53 gene delivery results in sustained antiproliferative activity in breast cancer cells.* Molecular Pharmaceutics, 2004. **1**(3): p. 211.
33. Kocbek, P., et al., *Targeting cancer cells using PLGA nanoparticles surface modified with monoclonal antibody.* Journal of Controlled Release, 2007. **120**(1-2): p. 18-26.
34. El-Sayed, M., A.S. Hoffman, and P.S. Stayton, *Rational design of composition and activity correlations for pH-sensitive and glutathione-reactive polymer therapeutics.* Journal of Controlled Release, 2005. **101**(1-3): p. 47-58.
35. Panyam, J., et al., *Rapid endo-lysosomal escape of poly(DL-lactide-co-glycolide) nanoparticles: implications for drug and gene delivery.* The FASEB journal : official publication of the Federation of American Societies for Experimental Biology, 2002. **16**(10): p. 1217-1226.
36. Prabha, S. and V. Labhasetwar, *Critical determinants in PLGA/PLA nanoparticle-mediated gene expression.* Pharmaceutical research, 2004. **21**(2): p. 354-364.
37. Dayton, P.A., et al., *Application of ultrasound to selectively localize nanodroplets for targeted imaging and therapy.* Mol Imaging, 2006. **5**(3): p. 160-74.
38. Lum, A.F.H., et al., *Ultrasound radiation force enables targeted deposition of model drug carriers loaded on microbubbles.* Journal of Controlled Release, 2006. **111**(1-2): p. 128-134.
39. Crowder, K.C., et al., *Sonic activation of molecularly-targeted nanoparticles accelerates transmembrane lipid delivery to cancer cells through contact-mediated mechanisms: implications for enhanced local drug delivery.* Ultrasound in Medicine and Biology, 2005. **31**(12): p. 1693.
40. Frenkel, V., et al., *Delivery of liposomal doxorubicin (Doxil) in a breast cancer tumor model: investigation of potential enhancement by pulsed-high intensity focused ultrasound exposure.* Acad Radiol, 2006. **13**(4): p. 469-79.
41. Nightingale, K., et al., *Acoustic radiation force impulse imaging: in vivo demonstration of clinical feasibility.* Ultrasound Med Biol, 2002. **28**(2): p. 227-35.
42. Zambaux, M.F., et al., *MPEO-PLA nanoparticles: Effect of MPEO content on some of their surface properties.* Journal of Biomedical Materials Research, 1999. **44**(1): p. 109-115.
43. Insana, M. and M. Oelze, *Advanced ultrasonic imaging techniques for breast cancer research*, in *Emerging Technologies in Breast Imaging and Mammography*, J. Suri, R. Rangayyan, and L. S., Editors. 2006, American Scientific Publishers: Valencia CA.
44. Wheatley, M.A., et al., *Surfactant-stabilized contrast agent on the nanoscale for diagnostic ultrasound imaging.* Ultrasound in Medicine and Biology, 2006. **32**(1): p. 83.
45. Marsh, J., et al., *Molecular imaging with targeted perfluorocarbon nanoparticles: Quantification of the concentration dependence of contrast enhancement for binding to sparse cellular epitopes.* ULTRASOUND IN MEDICINE AND BIOLOGY, 2007. **33**(6): p. 950-958.

46. Streeter, J.E., et al., *Improving Sensitivity in Ultrasound Molecular Imaging by Tailoring Contrast Agent Size Distribution: In Vivo Studies.* Molecular Imaging. **9**(2): p. 87-95.
47. Xing, X., et al., *The ets protein PEA3 suppresses HER-2/neu overexpression and inhibits tumorigenesis.* Nat Med, 2000. **6**(2): p. 189-95.
48. Shou, J., et al., *Mechanisms of tamoxifen resistance: increased estrogen receptor-HER2/neu cross-talk in ER/HER2-positive breast cancer.* Journal of the National Cancer Institute, 2004. **96**(12): p. 926.
49. Jerome, L., et al., *Recombinant human insulin-like growth factor binding protein 3 inhibits growth of human epidermal growth factor receptor-2-overexpressing breast tumors and potentiates herceptin activity in vivo.* Cancer Res, 2006. **66**(14): p. 7245-52.
50. Lanza, G.M., et al., *In vitro characterization of a novel, tissue-targeted ultrasonic contrast system with acoustic microscopy.* J Acoust Soc Am, 1998. **104**(6): p. 3665-72.
51. Lanza, G.M., et al., *High-frequency ultrasonic detection of thrombi with a targeted contrast system.* Ultrasound Med Biol, 1997. **23**(6): p. 863-70.
52. Liu, J., et al., *Nanoparticles as image enhancing agents for ultrasonography.* Physics in Medicine and Biology, 2006. **51**(9): p. 2179-2189.
53. Kaneda, M., et al., *Perfluorocarbon Nanoemulsions for Quantitative Molecular Imaging and Targeted Therapeutics.* Annals of Biomedical Engineering, 2009. **37**(10): p. 1922-1933.
54. Villanueva, F.S., *Molecular imaging of cardiovascular disease using ultrasound.* J Nucl Cardiol, 2008. **15**(4): p. 576-86.
55. Desai, M.P., et al., *The mechanism of uptake of biodegradable microparticles in Caco-2 cells is size dependent.* Pharm Res, 1997. **14**(11): p. 1568-73.
56. Athanasiou, K.A., G.G. Niederauer, and C.M. Agrawal, *Sterilization, toxicity, biocompatibility and clinical applications of polylactic acid/polyglycolic acid copolymers.* Biomaterials, 1996. **17**(2): p. 93-102.
57. Muller, W.J., et al., *Single-step induction of mammary adenocarcinoma in transgenic mice bearing the activated c-neu oncogene.* Cell, 1988. **54**(1): p. 105-15.
58. Kennecke, H., et al., *Metastatic Behavior of Breast Cancer Subtypes.* J Clin Oncol.
59. Jain, K.K., *Nanodiagnostics: application of nanotechnology in molecular diagnostics.* Expert Rev Mol Diagn, 2003. **3**(2): p. 153-61.
60. Hughes, M.S., et al., *Acoustic characterization in whole blood and plasma of site-targeted nanoparticle ultrasound contrast agent for molecular imaging.* The Journal of the Acoustical Society of America, 2005. **117**(2): p. 964-972.
61. Lanza, G.M., et al., *A novel site-targeted ultrasonic contrast agent with broad biomedical application.* Circulation, 1996. **94**(12): p. 3334.
62. Couture, O., et al., *A model for reflectivity enhancement due to surface bound submicrometer particles.* Ultrasound in Medicine and Biology, 2006. **32**(8): p. 1247.

63. Marsh, J.N., et al., *Improvements in the ultrasonic contrast of targeted perfluorocarbon nanoparticles using an acoustic transmission line model.* IEEE Trans Ultrason Ferroelectr Freq Control, 2002. **49**(1): p. 29-38.
64. Euliss, L.E., et al., *Imparting size, shape, and composition control of materials for nanomedicine.* Chemical Society Reviews, 2006. **35**(11): p. 1095.
65. Rolland, J.P., et al., *Direct fabrication and harvesting of monodisperse, shape-specific nanobiomaterials.* Journal of the American Chemical Society, 2005. **127**(28): p. 10096.
66. Chen, S., et al., *Efficient gene delivery to pancreatic islets with ultrasonic microbubble destruction technology.* Proc Natl Acad Sci U S A, 2006. **103**(22): p. 8469-74.
67. Bekeredjian, R., et al., *Ultrasound-targeted microbubble destruction can repeatedly direct highly specific plasmid expression to the heart.* Circulation, 2003. **108**(8): p. 1022-6.
68. Miller, D.L., et al., *Influence of contrast agent dose and ultrasound exposure on cardiomyocyte injury induced by myocardial contrast echocardiography in rats.* Radiology, 2005. **237**(1): p. 137.
69. Miller, D.L., C. Dou, and B.R. Lucchesi, *Cardiac arrhythmia and injury induced in rats by burst and pulsed mode ultrasound with a gas body contrast agent.* Journal of ultrasound in medicine : official journal of the American Institute of Ultrasound in Medicine, 2009. **28**(11): p. 1519.
70. Panyam, J. and V. Labhasetwar, *Dynamics of Endocytosis and Exocytosis of Poly(D,L-Lactide-co-Glycolide) Nanoparticles in Vascular Smooth Muscle Cells.* Pharmaceutical research, 2003. **20**(2): p. 212-220.
71. Diaz-Lopez, R., et al., *The performance of PEGylated nanocapsules of perfluorooctyl bromide as an ultrasound contrast agent.* Biomaterials. **31**(7): p. 1723-31.
72. Fonseca, C., *Paclitaxel-loaded PLGA nanoparticles: preparation, physicochemical characterization and in vitro anti-tumoral activity.* Journal of controlled release : official journal of the Controlled Release Society, 2002. **83**(2): p. 273.
73. Xu, P., et al., *Intracellular drug delivery by poly(lactic-co-glycolic acid) nanoparticles, revisited.* Mol Pharm, 2009. **6**(1): p. 190-201.
74. Davda, J. and V. Labhasetwar, *Characterization of nanoparticle uptake by endothelial cells.* Int J Pharm, 2002. **233**(1-2): p. 51-9.
75. Richards, M.A., et al., *The influence on survival of delay in the presentation and treatment of symptomatic breast cancer.* Br J Cancer, 1999. **79**(5-6): p. 858-64.
76. Abbey, C.K., et al., *In vivo positron-emission tomography imaging of progression and transformation in a mouse model of mammary neoplasia.* Proc Natl Acad Sci U S A, 2004. **101**(31): p. 11438-43.
77. Dayton, P.A., et al., *Ultrasonic analysis of peptide- and antibody-targeted microbubble contrast agents for molecular imaging of alphavbeta3-expressing cells.* Mol Imaging, 2004. **3**(2): p. 125-34.

78. Ntziachristos, V. and B. Chance, *Probing physiology and molecular function using optical imaging: applications to breast cancer.* Breast Cancer Res, 2001. **3**(1): p. 41-6.
79. Caruthers, S.D., et al., *Anti-angiogenic perfluorocarbon nanoparticles for diagnosis and treatment of atherosclerosis.* Wiley Interdiscip Rev Nanomed Nanobiotechnol, 2009. **1**(3): p. 311-23.
80. Rapoport, N., Z. Gao, and A. Kennedy, *Multifunctional Nanoparticles for Combining Ultrasonic Tumor Imaging and Targeted Chemotherapy.* JNCI Journal of the National Cancer Institute, 2007. **99**(14): p. 1095-1106.
81. Ferrara, K., R. Pollard, and M. Borden, *Ultrasound microbubble contrast agents: fundamentals and application to gene and drug delivery.* Annu Rev Biomed Eng, 2007. **9**: p. 415-47.
82. Vasir, J.K. and V. Labhasetwar, *Quantification of the force of nanoparticle-cell membrane interactions and its influence on intracellular trafficking of nanoparticles.* Biomaterials, 2008. **29**(31): p. 4244-52.
83. Morse, P.M. and K.U. Ingard, *Theoretical Acoustics*. 1968: McGraw-Hill Book Company.
84. Rupper, A. and J. Cardelli, *Regulation of phagocytosis and endo-phagosomal trafficking pathways in Dictyostelium discoideum.* Biochim Biophys Acta, 2001. **1525**(3): p. 205-16.